The Cosmology of the Instant Reconstruction of the Path of Light

Vincenzo Peluso[*]
Present address: Via don Bosco, 11 00045 Genzano di Roma, Rome Italy

ABSTRACT

A new cosmological model is presented, with characteristics and trends very similar to those of the standard model, but without dark energy. It differs from the standard one essentially for a constant of integration, which derives from a hypothesis at the centre of this work, which gives rise to an extra spatial distance and an extra fictitious component of matter. Due to these extra parts, the density parameter of matter is no longer constant but increases from 0.5 to 1 from the beginning of time to the present day, although the universe is homogeneous and isotropic, and although the total amount of energy and matter are constant. Consequently, the new model, which has one less parameter, satisfies all the constraints arising from the current accurate measurements of the BAO and the angular power spectrum of the CMB with the values of the density parameters of matter which, according to the theory, apply in each context. Analogously, it solves the Hubble tension and the primordial lithium problem, although it introduces a deuterium problem. Finally, it shows that it is the pressure of matter due to its variability, not dark energy, that drives the current acceleration phase of the expansion of the universe started by $z \simeq 0.5099$, when the universe was 7.99 billion years old, about 5 billion years ago. On a small scale, the same hypothesis has very similar effects to the MOND theory and explains the rotational motion of galaxies.

Key words: Cosmology: theory – distance scale – cosmological parameters – primordial nucleosynthesis – dark matter – Galaxy: kinematics and dynamics

1 INTRODUCTION

The standard Big-Bang model of cosmology provides a successful framework in which to understand the thermal history of our Universe and the growth of cosmic structure, but it is essentially incomplete. It requires very specific initial conditions. It postulates a uniform cosmological background, described by a spatially-flat, homogeneous and isotropic Robertson-Walker (RW) metric, with scale factor $a(t)$. Within this setting, it also requires an initial almost scale-invariant distribution of primordial density perturbations as seen, for example, in the cosmic microwave background (CMB) radiation, on scales far larger than the causal horizon at the time the CMB photons last scattered. To overcome the aforementioned requirements, it is necessary the introduction of the ad hoc hypothesis of inflation. Furthermore, according to the model, only few percent of the density in the Universe is provided by normal baryonic matter. The ΛCDM model requires two additional ad hoc components: a non-baryonic cold dark matter (CDM) and an even more mysterious dark energy, which makes up the rest.

The problem is that the crucial function of theories such as dark matter, dark energy and inflation —each in its own way tied to the big bang paradigm— is not to describe known empirical phenomena but rather to maintain the mathematical coherence of the framework itself while accounting for discrepant observations.

With the increase in experimental sensitivity, observational evidence for deviations from ΛCDM is, therefore, expected.

The agreement between the BBN (Big Bang Nucleosynthesis) and CMB (the angular power spectrum of Cosmological Microwave Background temperature anisotropies), since both constrain independently the cosmological parameters of the Standard model, is considered the strongest evidence in favour of the correctness of the standard model. Eg, the observed deuterium abundance (D/H) which in turn implies $\Omega_b h^2 (BBN)$ in very good agreement with $\Omega_b h^2 (CMB)$ deduced from the analysis of the angular power spectrum of the cosmic microwave background in the context of the standard model. Nevertheless, although, there is a good agreement between light element abundances (helium-4 and deuterium) deduced from observations and calculated in primordial nucleosynthesis, there remains a yet-unexplained discrepancy of ^7Li abundance higher by a factor of $\sim$ 3 when calculated theoretically. Recently, even the measure of the primordial abundance of Deuterium shows signs of discrepancy with respect to the expected value, giving rise to a further Deuterium Tension (Pitrou et al. 2021).

On the other hand, the CMB Planck constraints are model dependent, therefore changing the cosmological scenario we can end with different conclusions, and anomalies and tensions between Planck and other cosmological probes are present well above the 3 standard deviations. These discrepancies, as time goes on, have persisted and strengthened despite several years of accurate analyses. The most famous and persisting anomalies and tensions of the CMB are:

(i) the Hubble Tension (at 5σ) (Riess et al. 2021): In recent years, new measurements of the Hubble constant, the rate of universal expansion, suggested major differences between two independent methods of calculation which have huge implications for the validity

[*] E-mail: fmsv.peluso@alice.it

of cosmology's current standard model at the extreme scales of the cosmos.

(ii) the lensing amplitude A_L internal anomaly (at more than 2σ) (Addison et al. 2016) : although the Planck lensing measurement is compatible with the theoretical expectation $A_L = 1$, the distributions of A_L inferred from the CMB power spectra alone indicate a preference for $A_L > 1$. Tension at more than 2σ level is apparent in $\Omega_c h^2$ and derived parameters, including H_0, Ω_m, and σ_8.

(iii) the S_8 tension with cosmic shear data (at 3.2σ) (Di Valentino et al. 2021): A tension on $S_8 = \sigma_8 \sqrt{\Omega_m/0.3}$ between the Planck data in the ΛCDM scenario and KiDS+VIKING-450 and DES-Y1 combined together.

Furthermore, the model, which is remarkably successful on scales larger than a few Megaparsecs, faces challenges on smaller scales. The most difficult ones are related with the rotation in the inner parts of spiral galaxies.

1.1 Premise to the presentation of the hypothesis

The Schwarzschild's metric, found by K. Schwarzschild (1916), is the solution of the Einstein equations for a gravitational field possessing central symmetry (such a field can be produced by any centrally symmetric distribution of matter). It completely determines the gravitational field in vacuum produced by any centrally-symmetric distribution of masses. The metric gives the connection between the metric of real space, or proper coordinates, and the metric of the four-dimensional space-time or Schwarzschild's coordinates, outside the gravitational radius.

The Friedmann–Lemaître–Robertson–Walker (FLRW) solution was developed independently by the named authors in the 1920s and 1930s. It too, as well as the Schwarzschild's solution, requires space to be spatially isotropic, i.e. no preferred direction. In contrast, it is obtained using a very different set of additional conditions: that space is filled with matter that is characterized by its density and pressure, but nothing else (no stress, no viscosity, etc.; a so-called "perfect fluid"); and that it is homogeneous, i.e same everywhere, but it can change as a function of time.

As a consequence, while the Schwarzschild solution is static and demonstrates the limits placed on a static spherical body before it must collapse to a black hole (the Schwarzschild limit does not apply to rapidly expanding matter), the FLRW equations describe an expanding or contracting cosmos that is uniformly filled with matter-energy.

While the Schwarzschild's coordinates are observer dependent and correspond to an "accelerated" frame, like that of an observer held at a fixed spatial point in the surrounding spacetime, the FLRW comoving coordinates (including the cosmic time) are universal and play the same roles as those of an observer falling freely under the influence of that object.

Although The FLRW metric is an exact solution of Einstein's field equations of general relativity, it doesn't derive from Einstein's field equations: it follows from the geometric properties of homogeneity and isotropy, that is from the symmetry properties in the case of complete isotropy. In this special case of an isotropic space, the curvature properties are determined by just one constant which is the scalar curvature.

"To investigate the metric it is convenient to start from geometrical analogy, by considering the geometry of isotropic three-dimensional space as the geometry on a hypersurface known to be isotropic, in a fictitious four-dimensional space (This four-space is understood to have nothing to do with four-dimensional space-time). Such a space is a hypersphere; the three-dimensional space corresponding to this has a positive constant curvature." (Landau & Lifshitz 1971, pag 334)

It is possible to establish a spherical coordinate system, with inclination γ, on the spherical surface of Radius R_0 (R_0 is the "radius of curvature" of the Universe). Usually, these Spherical coordinates (R_0, $\gamma^\diamond$) are converted into cylindrical coordinates ($r^\diamond$, $h^\diamond$) which correspond to the cosmic coordinates (d_M, t). The resulting metric, that is the FLRW metric:

$$-ds^2 = -c^2 dt^2 + a(t)^2 \left(\frac{dr^2}{1 - r^2/R_0^2} + r^2 d\theta^2 + r^2 \sin^2\theta d\phi^2 \right) \quad (1)$$

or equivalently, since $r = R_0 \sin\gamma$,

$$-ds^2 = -c^2 dt^2 + a(t)^2 R_0^2 \left(d\gamma^2 + \sin^2\gamma \left(d\theta^2 + \sin^2\theta d\phi^2 \right) \right) \quad (2)$$

introduces a scale factor varying with time:

$$a(t) = \frac{\lambda_{emitted}}{\lambda_{received}} = \frac{1}{1+z} \quad (3)$$

However, since it evolves according to Einstein's field equations, the metric has an analytic solution to Einstein's field equations given by the Friedmann equations when the energy-momentum tensor is similarly assumed to be isotropic and homogeneous.

$$H^2 \equiv \left(\frac{\dot{a}}{a}\right)^2 = \frac{8\pi G}{3}\rho - \frac{kc^2}{a^2} + \frac{\Lambda c^2}{3} \quad (4)$$

$$\dot{H} + H^2 \equiv \frac{\ddot{a}}{a} = -\frac{4\pi G}{3}\left(\rho + \frac{3p}{c^2}\right) + \frac{\Lambda c^2}{3} \quad (5)$$

This metric and these equations are the basis of the standard big bang cosmological model including the current ΛCDM model and the proposed model.
The model proposed here, however, assumes that the universe is a IRPLS spacetime.

1.2 The IRPLS

The IRPLS (Instant Reconstruction of the Path of Light Spacetime) or (Intention Relationship's PLS) is only and not other than the reconstruction, starting from the present instant, of the path of the intermediaries of the interaction (i.e. the bosons) that takes place between two individuals in relationship. This is the same path as the light between two mirroring individuals: each one reflects and is reflected by the other recursively.

In fact, if we place a clock on each of the two individuals involved in the interaction, we can historically reconstruct distances and time intervals from the sequence of times that appears in the mirror image. If we denote by $s_n^\diamond = t_n^\diamond - t_{n-1}^\diamond$ the distance between the two individuals at time t_n, we discover (see fig. 3) that the historical reconstruction of the distance series forms a geometric progression

$$t^\diamond = s_0^\diamond + s_1^\diamond + s_2^\diamond + s_3^\diamond + \ldots = s_0^\diamond \left(1 + K^\diamond + K^{\diamond 2} + K^{\diamond 3} + \ldots\right) = \frac{s_0^\diamond}{1 - K^\diamond}$$

where $s_0^\diamond$ is the scale factor and $k = \cos^\diamond\gamma$ is the common ratio. Therefore

$$\Delta\lambda^\diamond = t^\diamond - t_{-1}^\diamond = s_0^\diamond \quad \text{and} \quad V^\diamond = \frac{\Delta\lambda^\diamond}{t^\diamond} = \frac{\overline{AB}}{\overline{0A}} = 1 - K^\diamond$$
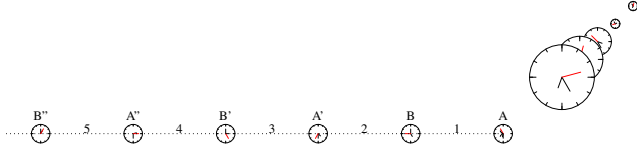
Figure 1. Recursive mirroring: two mirrors facing each other are reflected recursively. If there is a clock on each of them, in the reflected image present in every instant it is possible to reconstruct distances historically and therefore the velocities and accelerations over time, as far as the reflection allows.


Consummative Act: the element of the IRPLS
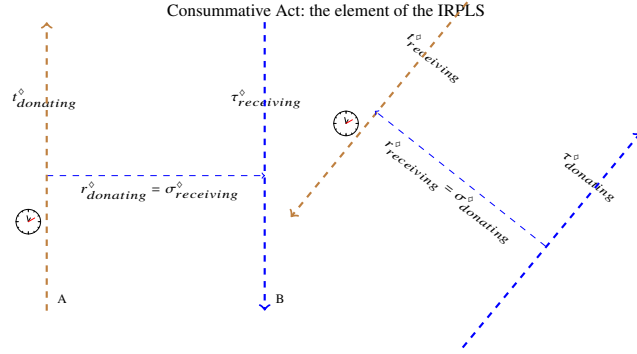
Figure 2. Consummative Act (not the event) is the element of the IRPLS: light does not have a speed, each segment of the path of light itself constitutes the space axis and determines the time axis, orthogonal to it, constituting the frames of the two individuals who oppose each other in the interaction. Consequently, for each individual, one frame corresponds to the act of giving and another frame corresponds to the act of receiving. The two frames are rotated to each other by a real γ angle. The determination of the γ angle is subject to the Uncertainty principle. Indeed, in a measurement, while the measuring instrument A is necessarily classic and therefore reflective, so we know $P^\diamond = t^\diamond_{A_i} - t^\diamond_{A_{i-1}}$, the measured B could be non-classic, therefore we would not know the proper time $t^\diamond_{B_i}$ and therefore we would not know

$$\cos \gamma^\diamond = \frac{t^\diamond_{B_i} - t^\diamond_{A_{i-1}}}{t^\diamond_{A_i} - t^\diamond_{B_i}}$$ and vice-versa.

Figure (3) compares the representation of the progression of events $A, B, A', B', \ldots$ in Minkowski's spacetime with that in IRPLS.

In contrast with the Minkowski's spacetime, in the IRPLS

• the individual manifests itself determined (particle) only in the act, i.e. only in the instant of giving/receiving energy, while it is in potency (wave function) otherwise. In other words, movement takes place not in act, but in the continuum of the potency which extends between one act and the next act of the relationship

• there is not a Time per se, other of space, the only dimension is the path of light in a relationship. Time is only the measure of the length of the total path of light. Light therefore does not have a speed and the metric is linear

• the element of the IRPLS is not the event, but the entire segment that unites the donor to the recipient (see fig. 2). Since light does not have a speed, each segment of the path of light itself constitutes the space axis and determines the time axis, orthogonal to it, constituting the frames of the two individuals who oppose each other in the interaction.

• Two frames corresponding to two successive acts of giving and receiving of a relationship form a γ angle between them. the IR-


The path of light in the recursive mirroring between A and B
Minkowski spacetime   *IRPLS (Path of Light Spacetime)*

$$\cos \gamma^\diamond_e = K^\diamond \qquad \sin \gamma^\diamond_e = 1 - K^\diamond$$
$$\cos \gamma^\diamond_i = -K^\diamond \qquad \sin \gamma^\diamond_i = 1 + K^\diamond$$

$$V^\diamond = \sin^\diamond \gamma = \frac{\lambda}{T} = \frac{x^\diamond_n}{t^\diamond_{0n}} = 1 - K^\diamond$$

$$r^2 = t^2 - \tau^2 \qquad\qquad x^\diamond_n = t^\diamond_n - t^\diamond_{n-1} \quad \text{or} \quad \Delta r^\diamond_{ab} = \sum_{n=a+1}^{b} x^\diamond_n$$
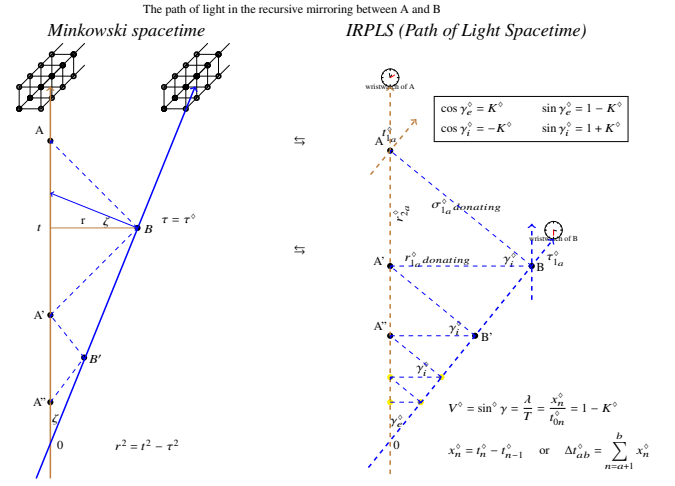
Figure 3. isomorphism: in comparison the representations of the geometric progression $A, B, A', B', A'', B'', \ldots$ with $K^\diamond(\gamma)$ as the common ratio, deriving from the recursive mirroring of individuals A and B (see fig. 1). The IRPLS diagram emerges from the historical reconstruction that connects the act of giving with the previous act of receiving and so on. Consequently, In the IRPLS diagram the homologous frames, and therefore the homologous axes, face each other forming an angle γ (the heterologous frames, and therefore the heterologous axes give-riceive are in fact always parallel to each other).

PLS represents the historical reconstruction of the relation donating-receiving of energy between two individuals starting from the current Act in the current instant. A reflective individual (i.e. a classic observer) extracts all the information from the image that reflexively emerges (i.e. from a sufficient number of concomitant acts) from and within the energy received.

In other words, it always represents a single instant: the entire spacetime of a relationship photographed in an instant

• the metric is linear $\Delta t^\diamond = \sum s^\diamond_i + R_i$. That is, time is the period of potency that extends between two acts and therefore is equal to the length of the path of light, which takes place partly in space and partly in the Radius (here the gravitational one)

• The circulation along a closed path is zero (zero curl). In a closed path, time is therefore the antilight, in the sense that it is of equal modulus and opposite sign to the light path.

• distance asymmetry: called $\overline{A'B}$ and $\overline{BA}$ the round trip of a signal between A and B, we have $\overline{A'B} = K^\diamond \overline{BA}$. Each segment of the path is $K^\diamond = \cos^\diamond \gamma$ times the previous one.

• the cipher of the linear geometry of the IRPLS diagram are the right Triangles $\triangle^\diamond_e$ and $\triangle^\diamond_i$, which correspond respectively to the rotation $\{\gamma_e \mid \sin^\diamond \gamma_e + \cos^\diamond \gamma_e = 1\}$ and $\{\gamma_i \mid \sin^\diamond \gamma_i + \cos^\diamond \gamma_i = 1\}$. In other words, there are two versions of the angle $\gamma^\diamond$

$$\cos \gamma^\diamond_e = K^\diamond(\gamma) \qquad\qquad \sin \gamma^\diamond_e = 1 - K^\diamond(\gamma) \qquad (6)$$
$$\cos \gamma^\diamond_i = -K^\diamond(\gamma) \qquad\qquad \sin \gamma^\diamond_i = 1 + K^\diamond(\gamma) \qquad (7)$$

It is easy to verify that:

$$\sin (\varphi_e \pm^\diamond \psi_e) = \sin^\diamond \varphi_e \pm \sin^\diamond \psi_e \qquad (8)$$
$$\cos (\varphi_e \pm^\diamond \psi_e) = \cos^\diamond \varphi_e \mp \sin^\diamond \psi_e \qquad (9)$$

The right Triangles $\triangle^\diamond_e$ and $\triangle^\diamond_i$ are the atoms and the compounds of the IRPLS diagram and they unfold recursively from each other alternating. Indeed, in a IRPLS diagram, each segment arises from a geometric progression which has as its common ratio $\cos^\diamond \gamma$ and as

scale factor a segment of a more primitive nature. Below the genesis of the spacetime (fig. 4):

• The genesis of the spacetime: *The core of a IRPLS diagram consists of the radius of the two interacting individuals linked by the path of light during their interaction. In the interaction, the light path cyclically connects the head of each radius with the tail of the opposite radius, crossing the same radii.*
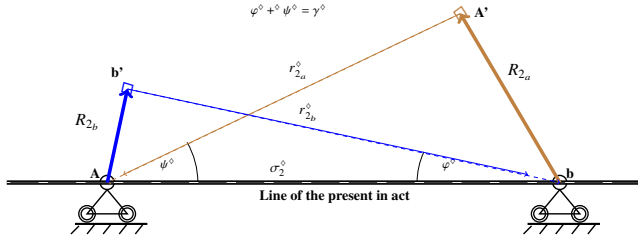
starting from the above schema, indicating with:

$$R_{2_a} = 2\frac{G}{c^2}M_a \qquad\qquad R_{2_{tot}} = R_{2_a} + R_{2_b}$$

Since for each observer A, its proper mass at rest is opposed to the remaining masses B placed in their centre of gravity and subjected to the total gravitational field, the global energy-momentum Radius of A and B is

$$R_{2_{Ab}}^\diamond = R_{2_a} + R_{2_b}\cos^\diamond\gamma \qquad\qquad R_{2_{Ba}}^\diamond = R_{2_b} + R_{2_a}\cos^\diamond\gamma$$

and since a round trip route passes through both A and B, it descends that space and time proceed from mass-energy as follows:

$$R_2^\diamond = \frac{R_{2_{Ab}}^\diamond + R_{2_{Ba}}^\diamond}{2} = \frac{R_{2_{tot}}(1+\cos^\diamond\gamma)}{2} = \frac{R_{2_{tot}}\sin^\diamond\gamma_i}{2} \qquad (10)$$

$$r_2^\diamond = \sum_{-\infty}^{0} R_{2_i}^\diamond = R_2^\diamond\left(1+\cos^\diamond\gamma+\cos^{\diamond 2}\gamma+\cdots\right) = \frac{R_2^\diamond}{\sin^\diamond\gamma_e} \qquad (11)$$

$$r^\diamond = \sum_{-\infty}^{0} r_{2_i}^\diamond = r_2^\diamond\left(1-\cos^\diamond\gamma+\cos^{\diamond 2}\gamma-\cdots\right) = \frac{r_2^\diamond}{\sin^\diamond\gamma_i} \qquad (12)$$

$$\tau^\diamond = \sum_{-\infty}^{0} r_i^\diamond = r^\diamond\left(1+\cos^\diamond\gamma+\cos^{\diamond 2}\gamma+\cdots\right) = \frac{r^\diamond}{\sin^\diamond\gamma_e} \qquad (13)$$

where

$$r_2^\diamond = \frac{r_{2_a}^\diamond + r_{2_b}^\diamond}{2} \qquad r^\diamond = \frac{r_a^\diamond + r_b^\diamond}{2} \qquad \tau^\diamond = \frac{\tau_a^\diamond + \tau_b^\diamond}{2}$$

At last, indicating with

$$R_x = \frac{R_{2_x}}{2} \qquad R_{tot} = \frac{R_{2_{tot}}}{2} = \frac{R_{2_a}+R_{2_b}}{2} = R_a+R_b = \frac{G}{c^2}(M_a+M_b)$$

from the eq. (10,11, 12, 13) descends the fundamental relation:

$$V^\diamond = \quad R_{tot} : r^\diamond = r^\diamond : \tau^\diamond = \sin^\diamond\gamma_e \quad = p^\diamond/m \qquad (14)$$

• geometry of the relation: in the instant the geometry is linear: A IRPLS closed polygonal chain corresponds, locally, to a manifold differential equation valid at that point.

• "principle of equivalence, in the instant, between inertial and not inertial systems": from the (14) the potential is equivalent to the momentum $V^\diamond \equiv p^\diamond/m$ and both correspond to a rotation, through a real angle $\gamma = \arcsin\left(V^\diamond\right)$, of the respective reference systems. The sine of the γ angle between rotating Radii (or any other pair of axes) corresponds to the potential or the momentum ($V^\diamond \equiv p^\diamond/m \equiv \sin^\diamond\gamma$). In the IRPLS space, therefore, there is no difference, in the instant, between an inertial and a non-inertial system, since both are
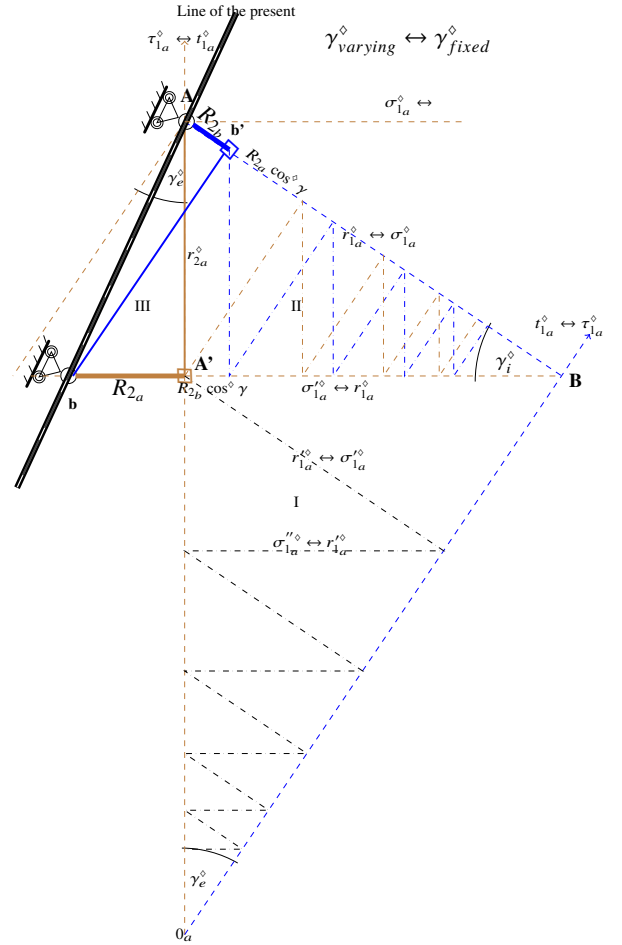

Figure 4. The whole relation is enfolded and unfolds from the Radii of the two conjoined individuals with the dual angles γ_e and γ_i alternating each other. It is governed by the relation $R : r^\diamond = r^\diamond : \tau^\diamond = \sin^\diamond\gamma$. Indeed the three quadrants represent time, space and Radius and recursively follow one another. In particular the III-II quadrants represent the internal energy-space plane, while the II-I quadrants the external space-time plane.
The diagram represents the historical reconstruction of the relationship starting from the current instant. It coincides with real history only when γ is constant.

characterized by a rotation angle γ. In an inertial system, in fact, the two radii are symmetrical and fictitious and translating (approaching or moving away) they do not rotate ($p^\diamond(\gamma)/m = r^\diamond/\tau^\diamond = const$) but their modulus grows as $R = V^\diamond r^\diamond$. On the other hand, in the gravitational or electrical interaction, the two Radii are real and their modulus is fixed and for both "freely falling" ≡ "rotating" : $V^\diamond(\gamma) = R_{tot}/r^\diamond$.

• The genesis of the three spatial dimensions: The genesis reported here, shows that space emerges from matter. In particular, matter is in three different states, each of the three dimensions emerges from one of the three states of matter:

(i) r_c from potency, that is CDM;
(ii) r_r from energy, that is radiation;
(iii) r_b from act, that is baryonic matter.

These three states of matter correspond to the three inner dimensions of space.

- the reflective birth of Euclidean geometry:

$$\mathbb{G}\left(\triangle_i^\diamond\right) \cdot \mathbb{G}\left(\triangle_e^\diamond\right) = \mathbb{G}\left(\triangle_{Euclid}\right) \quad \equiv$$
$$\left(\cos\gamma_i^\diamond + \sin\gamma_i^\diamond\right)\left(\cos\gamma_e^\diamond + \sin\gamma_e^\diamond\right) = \left(\cos\gamma^2 + \sin\gamma^2\right) \quad (15)$$

From the physical point of view, the (15) corresponds to the general energy-momentum relation both in the linear version and in the usual quadratic version. Indeed it's possible to show that for each physical equation, there are two dual forms, a linear one in the IRPLS plane and a quadratic one in the manifold.

- the isomorphism between SR, GTR and IRPLS.

From the previous definitions, differentials represent proper coordinates while segments represent reduced circumferences more or less the Radius.

Indeed, from fig. 4 and since, for the Schwarzschild coordinates, *"by definition, the "time" required by light to travel from A to B equals the "time" it requires to travel from B to A"* (Einstein 1905) we have:

$$d\tau = d\tau_1^\diamond \qquad\qquad d\sigma = d\sigma_1^\diamond \qquad (16)$$

$$r = \frac{\sigma_1^\diamond + r_1^\diamond}{2} = r^\diamond \pm \frac{R_{tot}}{2} = r^\diamond \pm R \qquad t = \frac{t_1^\diamond + t_1'^\diamond}{2} = t^\diamond \pm r \qquad (17)$$

Since in gravitation

$$K^\diamond = 1 - \sin\gamma \qquad\qquad \text{(in electricity } K^\diamond = \cos\gamma) \qquad (18)$$

defining $V^\diamond = \sin\gamma$, we have:

$$K_e^\diamond = K^\diamond \qquad\qquad\qquad K_i^\diamond = -K^\diamond \qquad (19)$$

$$V_e^\diamond = 1 - K^\diamond = V^\diamond \qquad\qquad V_i^\diamond = 1 + K^\diamond = 2 - V^\diamond \qquad (20)$$

and the (16, 17) become:

$$d\tau_e^\diamond = d\tau \qquad d\tau_i^\diamond = -d\tau \qquad d\sigma_e^\diamond = d\sigma \qquad d\sigma_i^\diamond = -d\sigma \qquad (21)$$

$$t_e^\diamond = t + r \qquad t_i^\diamond = t - r \qquad r_e^\diamond = r + R \qquad r_i^\diamond = r - R \qquad (22)$$

$$d\tau_x^\diamond = dt_x^\diamond\left(1 - V_x^\diamond\right)^k \qquad\qquad d\sigma_x^\diamond = \frac{dr_x^\diamond}{1 - V_x^\diamond} \qquad x = e, i \qquad (23)$$

where $k = 1$ when $d\gamma = 0$, $k = -1$ in a free falling frame ($d\gamma \neq 0$). Therefore, in a static frame ($dr = 0$ and therefore $dt_x^\diamond = dt$)

$$d\tau^2 = -d\tau_e^\diamond d\tau_i^\diamond = -dt_e^\diamond dt_i^\diamond\left(1 - V_e^\diamond\right)\left(1 - V_i^\diamond\right) = g_{00}\,dt^2 \qquad (24)$$

in a free falling frame ($dr \neq 0$)

$$d\tau_e^\diamond = \frac{dt_e^\diamond}{1 - V_e^\diamond} = \frac{\frac{E\,d\tau}{mc^2} - \frac{dr}{c}}{1 - V_e^\diamond} \qquad d\tau_i^\diamond = \frac{dt_i^\diamond}{1 - V_i^\diamond} = \frac{\frac{E\,d\tau}{mc^2} + \frac{dr}{c}}{1 - V_i^\diamond} \qquad (25)$$

$$d\tau^2 = d\tau_e^\diamond d\tau_i^\diamond = \frac{dt_e^\diamond dt_i^\diamond}{\left(1 - V_e^\diamond\right)\left(1 - V_i^\diamond\right)} = \frac{\frac{E^2}{m^2c^4}d\tau^2 - \frac{dr^2}{c^2}}{1 - 2V} \qquad (26)$$

$$\left(\frac{E^2}{m^2c^4} - 1\right) + 2V = \frac{dr^2}{c^2 d\tau^2} \qquad (27)$$

Since, from the above, it must be:

$$g_{00} = 1 - 2V \equiv -\left(1 - V_e^\diamond\right)\left(1 - V_i^\diamond\right) = \left(1 - V^\diamond\right)^2 = V_e^\diamond V_i^\diamond \qquad (28)$$

it follows that IRPLS physics is isomorphic to GTR via:

$$V \equiv \frac{V_e^\diamond V_i^\diamond}{2} = V^\diamond \frac{1 + \cos^\diamond \gamma}{2} = \frac{\frac{1}{2}R_2^\diamond}{r^\diamond} = V^\diamond\left(1 - \frac{V^\diamond}{2}\right) \qquad (29)$$

About the mapping between the angles ζ of Special Relativity and $\gamma^\diamond$, since, from the (22)

$$\begin{cases} t_1^\diamond = t + r = \tau_1^\diamond/\cos^\diamond \gamma \\[2mm] t_1'^\diamond = t - r = \tau_1^\diamond \cos^\diamond \gamma \end{cases} \implies \begin{cases} t_1^\diamond = \tau\cosh\zeta + \tau\sinh\zeta \\[2mm] t_1'^\diamond = \tau\cosh\zeta - \tau\sinh\zeta \end{cases}$$

we find that IRPLS physics is isomorphic to Special Relativity via:

$$e^{-\zeta} \equiv \cos^\diamond \gamma \qquad (30)$$

IRPLS physics, therefore, subsumes unifying Einstein's field equations and special relativity on a new ground.

1.3 The meaning of IRPLS and its relationship with Minkowski's spacetime

We saw in the previous paragraph that the physical representation in Minkowski/Riemannian manifold spacetime and that in the IRPLS, although completely different, as deriving from two completely different metaphysics, are isomorphic to each other. Which of the two is the real one (or the more primitive) is not a matter of taste, rather of criteria of naturalness, simplicity and generality.

According to the physicist John Wheeler, Einstein's general theory of relativity can be summed up in just 12 words: *"Space-time tells matter how to move; matter tells space-time how to curve"*.

IRPLS removes absolute spacetime: "matter tells matter how to move in the potency". More precisely, IRPLS also removes matter. In fact, the universe is the set of the totality of individuals in relation to each other where each individual (the elementary individual is the quantum of matter) is distinguished by its position with respect to the others.

The IRPLS diagram is only a knowledge representation system, it emerges reflexively (probabilistically) from the potency by means of the same theory on which QED is based, when the uncertainty inherent in IRPLS (see. fig. 2) dissolves. It is therefore the reality that lies beneath the Riemannian manifold that reflexively (phenomenologically) emerges from it, and the ground that unifies gravitation with quantum mechanics and inertial systems.

In Cosmology, it introduces a scale factor varying with time:

$$a(t) = K^\diamond = 1 - \sin\gamma = \frac{\lambda_{emitted}}{\lambda_{received}} = \frac{1}{1+z} \quad \left(\gamma = \arcsin\frac{z}{z+1}\right) \qquad (31)$$

path of light
cylindrical coordinates

$$r^\diamond + h^\diamond = R_0 \qquad a(t) = 1 - \sin\gamma \qquad (32)$$
$$r^\diamond = \sin\gamma R_0 \qquad h^\diamond = (1 - \sin\gamma)R_0 \qquad (33)$$
$$dr^\diamond = -R_0\,da \qquad dh^\diamond = R_0\,da \qquad (34)$$
$$dd_M = dr^\diamond/A \qquad c\,dt/a = dh^\diamond/A \qquad (35)$$

where $A = da/d\gamma$ is the curvature factor due to the non-zero energy density. From the definition:

$$A = \sqrt{1 - r^2/R_0^2} \quad \text{in the euclidean geometry} \qquad (36)$$
$$A^\diamond = 1 - r^\diamond/R_0 = a \quad \text{on the path of light.} \qquad (37)$$
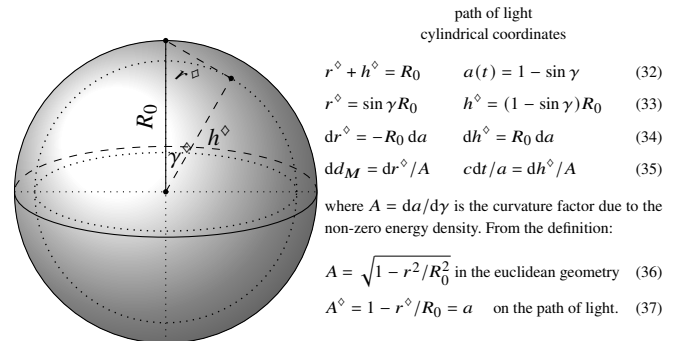
$$v = \tanh\zeta = \frac{r}{\tau\left(1 - V^\diamond\right) + r} = \frac{1 - \left(1 - \sin\gamma^\diamond\right)^2}{1 + \left(1 - \sin\gamma^\diamond\right)^2} = \frac{1 - K^{\diamond 2}}{1 + K^{\diamond 2}}$$

Therefore, we have the equivalence of the three redshifts:

Gravitational redshift $\dfrac{1}{1 - \frac{R_{tot}}{r^\diamond}} = \dfrac{1}{1 - V^\diamond} \qquad = \dfrac{1}{1 - \sin\gamma} = 1 + z$

Doppler redshift $\sqrt{\dfrac{1+v}{1-v}} = \dfrac{1}{K^\diamond} \qquad = \dfrac{1}{1 - \sin\gamma} = 1 + z$

FLRW redshift $\dfrac{t^\diamond}{\tau^\diamond} = \dfrac{\sigma^\diamond}{r^\diamond} = \dfrac{R_0}{h^\diamond} = \dfrac{1}{a} \qquad = \dfrac{1}{1 - \sin\gamma} = 1 + z$

In the next paragraphs we will see that it solves all the difficulties of current cosmology.

1.4 The hypothesis

The universe is the relationship of the whole with its parts from which the IRPLS emerges. Nevertheless, thanks to the isomorphism between the IRPLS and GTR, in the following we use the GTR by making the necessary additions in the form of hypotheses. Consequently, the following discussion is based on Einstein's field equations and Friedmann equations and FLRW metric with the addition of a hypothesis, that is: the distance measurements inside the Universe differ from those predicted by the standard model due to an integration constant.

Indeed, indicating with:

- $R_m(\gamma) = G/c^2 M(\gamma) = r_s/2$ one half of the Schwarzschild radius of the matter of the universe at a distance $r(\gamma)$
- R_Ω the constant gravitational Radius of the Universe, i.e. the constant total amount of matter-energy of the universe
- $R_{(t)} = c/H_{(t)}$ the Radius of curvature of the Universe, i.e. the positive curvature of the hypersphere corresponding to the Universe (At the present time, i.e. the current time which corresponds to cosmic time t_0 and to the Hubble constant H_0 and curvature Radius $R_0 = c/H_0$)

and defining "Cosmic Potential" and "Path of light in space" (distinct from the path of light in the Radius) as follows:

$$V^\diamond_{(\gamma)} = 1 - K^\diamond = \sin\gamma \qquad \text{"Cosmic Potential"} \qquad (38)$$

$$r^\diamond_{(\gamma)} = V_{(\gamma)} R_0 = \sin\gamma\, R_0 \qquad \text{"Path of light in space"} \qquad (39)$$

the IRPLC model makes the following general hypothesis:

Hypothesis 1 *The radial coordinate r[1] between two interacting (gravitationally) bodies (like the observer and the observed) is equal not only to the path of light in space $r^\diamond_{(\gamma)}$, but also, for each of them, to the length of their own gravitational radius R_m, and this, in a homogeneous and isotropic universe, due to the presence of dark matter as well as ordinary matter and radiation, increase proportionally to the square of the spatial distance (or as the Cosmic Potential times the Path of light in space). More precisely, we have:*

$$V^\diamond = R_m : r^\diamond = r^\diamond : \tau^\diamond = p^\diamond/m = \sin^\diamond\gamma \qquad (40)$$

$$r_{(\gamma)} = \int dr^\diamond_{(\gamma)} = r^\diamond_{(\gamma)} + C = r^\diamond_{(\gamma)} + R_{\mathbf{m}(\gamma)} = \mathbf{b}_\Gamma\, r^\diamond_{(\gamma)} \qquad (41)$$

(Cosmology begins when, in the 40, $\tau^\diamond = \tau^\diamond_{max} = R_0$)

We introduce, therefore, the cosmological factor[2] $\mathbf{b}_\Gamma \equiv \left(1 + \frac{R_m}{r^\diamond}\right) = \left(1 + \frac{R_\Omega}{R_0}\sin\gamma\right)$. Since the actual (or observed) density is equal to the critical density of the Friedmann universe

$$R_\Omega = R_0 = \frac{c}{H_0} \qquad \rightarrow \qquad \mathbf{b}_\Gamma = (1 + \sin\gamma) \qquad (42)$$

It is a parameter dependent only on the Path of light in space between the observed B and the observer A, and is constant along the entire path, being the equivalent of an integration constant.
We have, from the hypothesis:

$$R_{\mathbf{m}(\gamma)} = V_{(\gamma)}\, r^\diamond_{(\gamma)}\, \frac{R_\Omega}{R_0} = V_{(\gamma)}\, r^\diamond_{(\gamma)} \qquad (43)$$

$$r_{(\gamma)} = \int dr^\diamond_{(\gamma)} = r^\diamond_{(\gamma)} + C = r^\diamond_{(\gamma)} + R_{\mathbf{m}(\gamma)} = \mathbf{b}_\Gamma\, r^\diamond_{(\gamma)} \qquad (44)$$

Accordingly, for the line element:

$$dl^2 = \left(\frac{dr^2}{1 - r^2/R_0^2} + r^2 d\Omega^2\right) = \mathbf{b}_\Gamma^2\, R_0^2\left(d\gamma^2 + \sin^2\gamma\, d\Omega^2\right) \qquad (45)$$

At last, for the cosmic matter-energy

$$R_{\mathbf{ms}(\gamma)} = V_{(\gamma)}\, r_{(\gamma)} = \mathbf{b}_\Gamma R_{\mathbf{m}(\gamma)} = R_{\mathbf{m}(\gamma)} + R_{\mathbf{s}(\gamma)} \qquad (46)$$

although the average density is equal to the critical one, and therefore the universe is flat, the extra radius $R_{\mathbf{s}(\gamma)}$ of eq. 46, behaves like a vanishing mass that generates a radius of curvature R_0. As a result, the density of matter is no longer constant but increases from 0.5 to 1 from the beginning of time to the present day, although the universe is homogeneous and isotropic, and although the total amount of energy and matter are constant.

In the context of a Friedman-type model, in which the cosmos expands outward from a singularity, a time-varying scale factor $a(t)$ is introduced, as usual:

$$R_\Omega = R_\Omega \qquad R_{(t)} = a(t)\, R_0 \qquad r_{(\gamma,t)} = a(t)\, r_{(\gamma)} \qquad (47)$$

It is important to underline that the IRPLC hypothesis, which conforms to the law of conservation of energy and to the principle of homogeneity (no privileged points) and isotropy of the universe, does not change the FLRW metric, nor the Einstein's field equations, nor Friedmann's equations. Consequently, the cosmic volume must correspond to the wedge of the universe that goes from the singularity of the Big Bang to the space surface at time t

$$Vol_{(r_{(\gamma,t)})} = \frac{4}{3}\pi r^2_{(\gamma,t)}\, a(t)\, R_0 = \sin^2\gamma\, \frac{4}{3}\pi\,(a(t)R_0)^3 \qquad (48)$$

so that :

$$\rho_{\mathbf{ms}(t)} = \frac{c^2}{2\,G}\frac{R_{\mathbf{ms}(\gamma)}}{Vol_{(r_{(\gamma,t)})}} = \frac{3H_0^2}{8\pi G}\frac{\mathbf{b}_\Gamma\,\Omega_m}{a(t)^3} \qquad (49)$$

(note that the different definitions of volume (eq.48) and density (eq.49) do not alter the Friedmann fluid equation)
where the matter density, together with its radiant component, is equal to the critical density $\Omega_r + \Omega_m = 1$ where $\Omega_m = \Omega_b + \Omega_c$

$$R_\Omega = R_{\Omega_r} + R_{\Omega_b} + R_{\Omega_c} \qquad \equiv \qquad 1 = \Omega_r + \Omega_b + \Omega_c \qquad (50)$$

Given the relationship between space and mass-energy (see eq.

---

[1] r is gotten by dividing the measured circumference of a circle by 2π

[2] on the small scale, the cosmological factor is negligible: one astronomical unit corresponds to $\sin\Gamma(1au) \simeq 1.2 \times 10^{-15}$.

46), it is possible to break down the elements of the metric according to the type of energy

$$\frac{1}{R_0^2} = \frac{1}{R_{0_r}^2} + \frac{1}{R_{0_b}^2} + \frac{1}{R_{0_c}^2} = \frac{\Omega_r}{R_0^2} + \frac{\Omega_b}{R_0^2} + \frac{\Omega_c}{R_0^2} \tag{51}$$

$$\frac{1}{dr^2} = \frac{1}{dr_r^2} + \frac{1}{dr_b^2} + \frac{1}{dr_c^2} = \left(\frac{1}{R_{0_r}^2} + \frac{1}{R_{0_b}^2} + \frac{1}{R_{0_c}^2} \right) \frac{1}{(d \sin \gamma)^2} \tag{52}$$

$$\frac{1}{dd_M^2(z)} = \frac{1}{dd_{M_r}^2(z)} + \frac{1}{dd_{M_b}^2(z)} + \frac{1}{dd_{M_c}^2(z)} = \frac{H^2(z)}{c^2 dz^2} \tag{53}$$

$$H^2(z) = H_r^2(z) + H_b^2(z) + H_c^2(z) \tag{54}$$

In details:

Energy kind	FLRW coordinates	ΛCDM model	IRPLC model
r	$dd_{M_r} = \frac{dr_r}{A_r}$	$-R_{0_r}\, da$	$-R_{0_r}\, da$
b	$dd_{M_b} = \frac{dr_b}{A_m}$	$R_{0_b}\sqrt{1+\sin\gamma}\, d\gamma$	$b_\Gamma R_{0_b} d\gamma$
c	$dd_{M_c} = \frac{dr_c}{A_m}$	$R_{0_c}\sqrt{1+\sin\gamma}\, d\gamma$	$b_\Gamma R_{0_c} d\gamma$
Λ	$dd_{M_\Lambda} = \frac{dr_\Lambda^\diamond}{A_\Lambda}$	$R_{0_\Lambda}\, dz$	0

$$\text{(55)}$$

where $A_r = 1$ $A_m = \sqrt{1 - r^2/R_0^2} = \cos\gamma$ $A_\Lambda = a^2$

In the (55), each component dd_{M_x} was deduced: by means of backward reasoning starting from the *Metric* (60), for the ΛCDM model; according to (Landau & Lifshitz 1971, pag. 333-336) and Hypothesis (1), for the IRPLC model. Since

$$d_{M_m}(\gamma)/R_{\omega_m} = b(\Gamma) \int_0^\gamma d\gamma = b(\Gamma)\gamma = (1 + \sin\gamma)\,\gamma \tag{56}$$

$$d'_{M_m}(\gamma)/R_{\omega_m} = 1 + \sin\gamma + \gamma\cos\gamma \tag{57}$$

$$dz = -\frac{da}{a^2} = \frac{\cos\gamma}{a^2}\,d\gamma = \sqrt{(1 + \sin\gamma)a^{-3}}\,d\gamma \tag{58}$$

$$\frac{c}{H_x} = d'_{M_x}(z) = 1/\sqrt{\frac{(1+\sin\gamma)a^{-3}}{\left(d'_{M_x}(\gamma)\right)^2}} \tag{59}$$

we have at last

model	Metric
ΛCDM	$d_M = \displaystyle\int_0^z \frac{c\, dz}{H_0 \sqrt{\frac{\Omega_r}{a^4(t)} + \frac{\Omega_m}{a^3(t)} + \Omega_\Lambda}}$
IRPLC	$d_M = \displaystyle\int_0^z \frac{c\, dz}{H_0 \sqrt{\frac{\Omega_r}{a^4(t)} + \frac{1+\sin\gamma}{(1+\sin\gamma+\gamma\cos\gamma)^2}\frac{\Omega_m}{a^3(t)}}}$

$$\text{(60)}$$

As for the IRPLC Hubble parameter, from the eq. (60) we have:

$$H(a) = H_0 \left[\frac{\Omega_r}{a^4(t)} + \frac{\Omega_{ms}(\gamma)}{a^3(t)} \right] \tag{61}$$

$$\Omega_{ms}(\gamma) = \frac{1+\sin\gamma}{(1+\sin\gamma+\gamma\cos\gamma)^2}\,\Omega_m = \Omega_m(\gamma) + \Omega_s(\gamma) \tag{62}$$

The denominator of the eq. (62) derives (see eq. 57) from the extra path of light represented by the cosmological factor b_Γ. Regarding the numerator of the (62), while the first term represents the proper mass due to to the path of light in space $r^\diamond$, the second term, characteristic and distinctive of the IRPLC model compared

to the standard one, represents the extra mass due to extra distance constituted by the length of the Radius (i.e. to the extra path). We will indicate this second term, i.e. Ω_s, with the name of "shadow matter". It is assumed to be a fictitious mass of a different nature from proper mass.

The cosmological factor b_Γ has important consequences on the metric and constitutes the original difference compared to the ΛCDM model. In fact, it implies that, although the total amount of energy and matter in the Universe remains constant, space varies instead with a law different from the simple cube of distance.
Nevertheless the extra distance and the extra mass given by the cosmological factor b_Γ are fictitious and give rise to a fictitious curvature. Consequently, although the universe is locally flat $\Omega_r + \Omega_m = 1$, it is finite and has a positive spatial curvature (spherical). Indeed, the "shadow matter" breaks down into two components:

$$\Omega_s(\gamma) = \frac{1 - 1 + \sin\gamma}{(1+\sin\gamma+\gamma\cos\gamma)^2}\,\Omega_m = \Omega_h(\gamma) + \Omega_k(\gamma)\,a(\gamma) \tag{63}$$

We can therefore rewrite the eq. (61) as follows:

$$H(a) = H_0 \left[\frac{\Omega_r}{a^4(t)} + \frac{\Omega_m(\gamma)}{a^3(t)} + \frac{\Omega_h(\gamma)}{a^3(t)} + \frac{\Omega_k(\gamma)}{a^2(t)}\frac{a(\gamma)}{a(t)} \right] \tag{64}$$

where

$$\Omega_m(\gamma) = \frac{1}{(1+\sin\gamma+\gamma\cos\gamma)^2}\,\Omega_m \tag{65}$$

$$\Omega_h(\gamma) = \frac{1}{(1+\sin\gamma+\gamma\cos\gamma)^2}\,\Omega_m \tag{66}$$

$$\Omega_k(\gamma) = \frac{-1}{(1+\sin\gamma+\gamma\cos\gamma)^2}\,\Omega_m \tag{67}$$

Since along the line of sight $a(\gamma) = a(t)$, the universe appears endowed with a fictitious positive curvature. Nevertheless, the universe is flat in itself as cosmological observations reveal.

Analogously, the cosmological factor b_Γ gives rise to a fictitious matter pressure and therefore to the acceleration in the expansion of the universe. Indeed, starting from the above density formulas, since, using the first equation (4), the second equation (5) can be re-expressed as:

$$\dot\rho = -3\frac{\dot a}{a}\left(\rho + \frac{p}{c^2}\right) \quad\text{or}\quad \frac{p}{c^2} = -\left(\frac{1}{3}\frac{a}{\dot a}\dot\rho + \rho\right) \tag{68}$$

and since, from the (1), $d\tau = a d'_M(\gamma)d\gamma$ and $da = -\cos\gamma d\gamma = H_0\, dr$, we have:

$$\frac{\dot a}{a} = H_0 \frac{1}{a^2}\frac{dr}{dd_M} = \sqrt{\frac{8\pi G}{3}\rho} \tag{69}$$

$$\frac{p_r(t)}{c^2} = \rho_{crit}\frac{1}{3}\Omega_r a_{(t)}^{-4} \tag{70}$$

$$\frac{p_m(t)}{c^2} = \frac{2}{3}\frac{1}{\cos\gamma}\frac{\gamma\sin\gamma - 2\cos\gamma}{1+\sin\gamma+\gamma\cos\gamma}a_{(t)}\rho_m(t) \tag{71}$$

$$\frac{p_s(\gamma)}{c^2} = \frac{p_m(\gamma)}{c^2}(1 - a(\gamma)) + \frac{1}{3}a_{(\gamma)}\rho_m(\gamma) \tag{72}$$

When $t \to t_0$, that is $\gamma \to 0$ or $a(t) = a(\gamma) \to 1$, we have that the proper matter pressure becomes negative:

$$\lim_{t\to t_0}\frac{p_m(t)}{c^2} = -\rho_m(t_0)$$

and, from the (5), the acceleration in the expansion of the universe becomes positive:

$$\lim_{t\to t_0}\ddot a_{(t)} = \frac{8\pi G}{3c^2}\rho_m(t_0) = \frac{R_\Omega}{R_0^3} = (cH_0)^2$$

The purpose of this article is to demonstrate that the IRPLC cosmology finally satisfies all constraints deriving from cosmological observations.

2 IMPACTS OF THE IRPLC HYPOTHESIS ON STANDARD COSMOLOGY

Since $\Omega_c = 1 - \Omega_r - \Omega_b$, the IRPLC Model is determined by only five of the six parameters of the ΛCDM model:

$$\omega_{b_0}, h, n_s, \tau, N_{eff} \tag{73}$$

At last, since the radiation density is precisely determined by the CMB temperature and by the physics of the standard model, the metric of the IRPLC Model (eq. 60) is determined by a single parameter:

$$\mathcal{M}(H_0)$$

About the shadow matter, being a fictitious mass, it intervenes in the IRPLC metric but does not contribute to the speed of sound, nor does it contribute to the extra inertia in the evolution of the acoustic wave oscillation.

As densities vary with redshift, it is important to bear in mind that, unlike the ΛCDM model, in the IRPLC model we must use the appropriate value of the density of matter according to the context.

In order to highlight the actual causal region on a case-by-case basis, we introduce the functions $f_m(z) = \Omega_m(z)/\Omega_{m_0}$, $f_s(z) = \Omega_s(z)/\Omega_{m_0}$ and $f_{ms}(z) = f_m(z) + f_s(z)$. Therefore:

• acoustic waves dynamic: CMB temperature and polarization anisotropies are determined not only by the metric but also by the speed of acoustic wave and by the Baryon drag which depend only on the matter component.

$$c_s(z) \equiv c \sqrt{\frac{\dot{P}_\gamma + \dot{P}_b}{\dot{\rho}_\gamma + \dot{\rho}_b}} \simeq \frac{c}{\sqrt{3}} \frac{1}{\sqrt{1 + f_m(z)\frac{3\Omega_{b_0}}{4\Omega_\gamma(1+z)}}} \tag{74}$$

The causal region, however, differs between the two cases:

– speed of acoustic wave c_s : the causal region is given by the cosmological redshift

$$1 + R(z) = 1 + f_m(z)\frac{3\,\Omega_{b_0}}{4\,\Omega_\gamma(1+z)} \tag{75}$$

– Baryon Loading: momentum density provides extra inertia in the joint Euler equation for the evolution of acoustic wave oscillation. In this case, the causal region is restricted to the distance between baryons with respect to their barycentre given by the angle $\theta_z \equiv r_s(z)/D_M(z)$

$$m_{eff} = 1 + R(\theta_z) = 1 + f_m(\theta_z)\frac{3\,\Omega_{b_0}}{4\,\Omega_\gamma(1+z)} \tag{76}$$

• BBN: while both the expansion rate of the universe during the BBN and the baryon-to-photon ratio η are the same for ΛCDM and IRPLC model, the baryon density of IRPLC model is almost exactly one half with respect to ΛCDM model

$$\rho_{bs}(z_{BBN}) = f_{ms}(z_{BBN})\Omega_{b_0}(1+z)^3 \simeq \frac{1}{2}\Omega_{b_0}(1+z)^3 \tag{77}$$

consequently, the nuclear reaction rate of the IRPLC model is half that of the ΛCDM model.
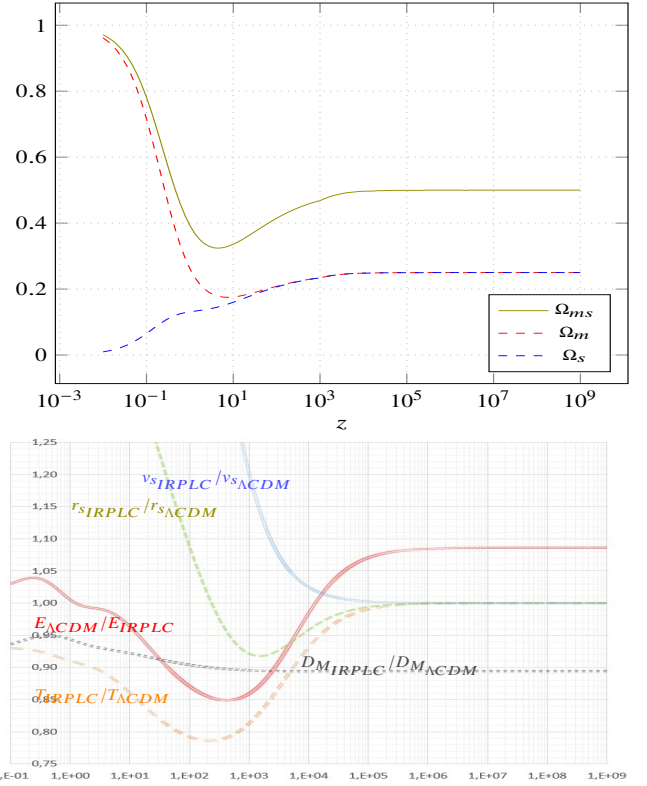

Figure 5. on the top panel, the density of matter and its two components as a function of the redshift.
On the bottom panel, the scale ratio between the fiducial ΛCDM model ($\omega_b = 0.02242$, $\omega_m = 0.3111$, $H_0 = 67.66$) and the IRPLC Model ($\omega_b = 0.02325$, $H_0 = 73.48$). The two models thus configured give rise to an almost identical BAO "Hubble diagram"' (fig. 11)

About the history of the universe, both models basically share the same phases.
In the Radiation-dominated age, although the nucleosynthesis and the dynamics of the acoustic oscillation are different, the expansion rate: $H(a) \simeq H_0 \sqrt{\frac{\Omega_r}{a^4}}$ is identical for both models.
Unlike the ΛCDM model, in the IRPLC model we can distinguish between two radiation matter transitions:

(i) The Radiation-MatterShadow transition happened when $H_r = H_{ms}$, or $d'_{M_{ms}} = d'_{M_r}$, that is $\Omega_{ms}(z) = \Omega_r(1+z)$ or:

$$\left(\frac{\cos\gamma\left(z_{eq_{ms}}\right)}{1 + \sin\gamma(z_{eq_{ms}}) + \gamma(z_{eq_{ms}})\cos\gamma(z_{eq_{ms}})}\right)^2 = \frac{\Omega_r}{1 - \Omega_r} \tag{78}$$

(ii) The Radiation-Matter transition happened when $H_r = H_m$, or $d'_{M_m} = d'_{M_r}$, that is $\Omega_m(z) = \Omega_r(1+z)$ or:

$$\frac{1 - \sin\gamma\left(z_{eq_m}\right)}{\left(1 + \sin\gamma(z_{eq_m}) + \gamma(z_{eq_m})\cos\gamma(z_{eq_m})\right)^2} = \frac{\Omega_r}{1 - \Omega_r} \tag{79}$$

Contrary to what happens in the radiation dominate era, in the matter dominated era the expansion rate of the universe is quite different (fig. 5).
Furthermore, since there is no Dark Energy in the IRPLC model, the matter-dominated era extends to the present and thus encompasses the final era of accelerated expansion of the universe.

3 CONSTRAINTS ON IRPLC COSMOLOGICAL PARAMETERS

We determine the last three parameters of the IRPLC model and the radiation density as follows:

• The value of the number of effective relativistic degrees of freedom is (Mangano et al. 2005; de Salas & Pastor 2016; Grohs & Fuller 2017; Escudero Abenza 2020; Akita & Yamaguchi 2020; Froustey et al. 2020; Bennett et al. 2020)

$$N_{eff} = 3.044 \qquad (80)$$

for 3 neutrino families, taking into account the neutrino decoupling physics. This value is very robust and can be understood fully from the adiabatic transfer of averaged oscillations (ATAO) approximation (Froustey et al. 2020). This allows one to show that this prediction is insensitive to the type of neutrino mass hierarchy (normal or inverted) as it depends nearly exclusively on mixing angles. Also, since mixing angles are currently known with rather good precision, the propagation of uncertainty affects N_{eff} with $\pm 2 \times 10^{-5}$ only.

• CMB constraints on the scalar spectral index n_s, which describes how the density fluctuations from inflation vary with scale ($n_s = 1$ corresponding to scale invariant fluctuations) (Planck Collaboration et al. 2020)

$$n_s = 0.9649 \pm 0.0042 \qquad (81)$$

• CMB constraints on the reionization optical depth τ (Planck Collaboration et al. 2020)

$$\tau = 0.0544 \pm 0.0073 \qquad (82)$$

• the T_{cmb} constraint: $T_{cmb} = 2.7255 \pm 0.0006$ K (Fixsen 2009), implies that the photon density is $\Omega_\gamma = 2.469 \times 10^{-5} h^{-2}$ and therefore we can reduce the radiation density $\Omega_r = \Omega_\gamma \left(1 + 0.2271 N_{eff}\right)$ and matter density to a function of just the parameter H_0

$$\Omega_r = 2.469 \times 10^{-5} h^{-2} \left(1 + 0.2271 \cdot 3.044\right) \qquad (83)$$

$$\Omega_m = 1 - \Omega_r \qquad (84)$$

Furthermore, the remaining two parameters of the IRPLC model, i.e. the baryonic component of the matter density and the Hubble constant, must satisfy the following additional constraints:

(i) The acoustic angular scale constraint: The acoustic oscillations in l seen in the CMB power spectra correspond to a sharply-defined acoustic angular scale on the sky, given by:

$$\frac{\pi}{\ell_a} = \theta_* = \frac{r_s^*}{d_M} \qquad (85)$$

where $r_s^* = r_s(z^*)$ is the comoving sound horizon at recombination quantifying the distance the photon-baryon perturbations can influence, $d_M(z^*)$ is the comoving angular diameter distance that maps this distance into an angle on the sky, and z^* depends on the ionization history and the atomic physics of recombination. It is possible to determine z^* by using the accurate recombination fitting formulae (Hu & Sugiyama 1996). In this article, however, we have used the CAMB software [3], which provides very similar, but even more accurate results. *Planck* measures:

$$100\theta_* = 1.04109 \pm 0.00030 \quad \text{(68\%, TT,TE,EE+lowE)} \qquad (86)$$

a measurement with 0.03% precision.
Because of its simple geometrical interpretation, θ_* is measured very robustly and almost independently of the cosmological model.

---

[3] CAMB is available online at the following website:
https://lambda.gsfc.nasa.gov/toolbox/tb_camb_form.cfm

(ii) The BAO measurement constraint: The transverse baryon acoustic oscillation scale r_{drag}/d_M measured from galaxy surveys, where r_{drag} is the comoving sound horizon at the end of the baryonic-drag epoch, is the analogue of CMB acoustic angular scale.

The BAO measurement constraint can be expressed as a approximate relation between $r_{drag} = r_s(z_{drag})$ and h, where z_{drag} is the redshift at the drag epoch, as:

$$\left(\frac{r_{drag} h}{\text{Mpc}}\right)\left(\frac{0.3}{\Omega_m}\right)^{0.4} = 101.056 \pm 0.036 \qquad (87)$$

for the ΛCDM $\mathcal{M}$etric (Planck Collaboration et al. 2020)

$$\left(\frac{r_{drag} h}{\text{Mpc}}\right) = 101 \pm 1 \qquad (88)$$

for the $\mathcal{M}$etric of the present model (fig. 6).

(iii) "Late universe" H_0 measurements constraint: "Late universe" H_0 measurements using calibrated distance ladder techniques have converged on a value of approximately $H_0 \simeq 73.4$ km/s/Mpc. In particular, 73.4 ± 1.4 km/s/Mpc (Reid et al. 2019) from standard distance ladder, 73.3 ± 1.7 km/s/Mpc (Wong et al. 2020) from strong gravitational lensing effects on quasar systems.

(iv) the angular power spectrum of the CMB. At last, in addition to the constraints already expressed on the acoustic angular scale and on the scalar spectral index, the angular power spectrum of the CMB, within the assumptions underlying the standard model, provides precise measurements of the baryon density and dark matter density of the universe at recombination (Hu & Dodelson 2002). In particular, 2nd/1st peak ratio allows to determine the baryon density, one of the most robust and best-determined CMB outputs, since it controls the relative amplitudes of the alternating odd and even peaks, which correspond to modes undergoing maximal compression and rarefactions at the time of recombination.

The (Planck Collaboration et al. 2020), for the base-ΛCDM model from Planck CMB power spectra, in combination with CMB lensing reconstruction, finds, for TT,TE,EE+lowE+lensing 68% limits:

$$\omega_b = 0.02237 \pm 0.00015 \qquad (\omega_c = 0.1200 \pm 0.0012)$$

(v) BBN predictions and primordial element abundances measurement constraint. In the present article we have used the version 2 of the software AlterBBN [4] suitably modified to adapt it to the different nuclear reaction rates of the present model which are half of the standard ones. Indeed, $\rho_b(z_{BBN}) = 0.5\,\rho_{0_b}$.

(vi) the acceleration in the expansion of the universe determined by comparing the brightness or faintness of distant supernovae relative to the empty Universe model (Riess et al. 1998)

4 TESTING THE IRPLC MODEL

The z^* and z_{drag} depend on the ionization history taking into account the atomic physics of recombination at the last scattering and drag epochs respectively. Since it is important to achieve the highest level of accuracy, the CAMB software was used to determine z^*

---

[4] AlterBBN can be downloaded from the website: https://alterbbn.hepforge.org/ . It is an open public code for the calculation of the abundance of the elements from Big-Bang nucleosynthesis in alternative cosmological scenarios, in a fast and reliable way. For the purpose of the IRPLC model, the *bbnrate.c* file was modified by adding the instruction " **f[ie]=0.5*f[ie]**;" at the end of the loop of the *rate_all* function in order to halve all the reaction rates.
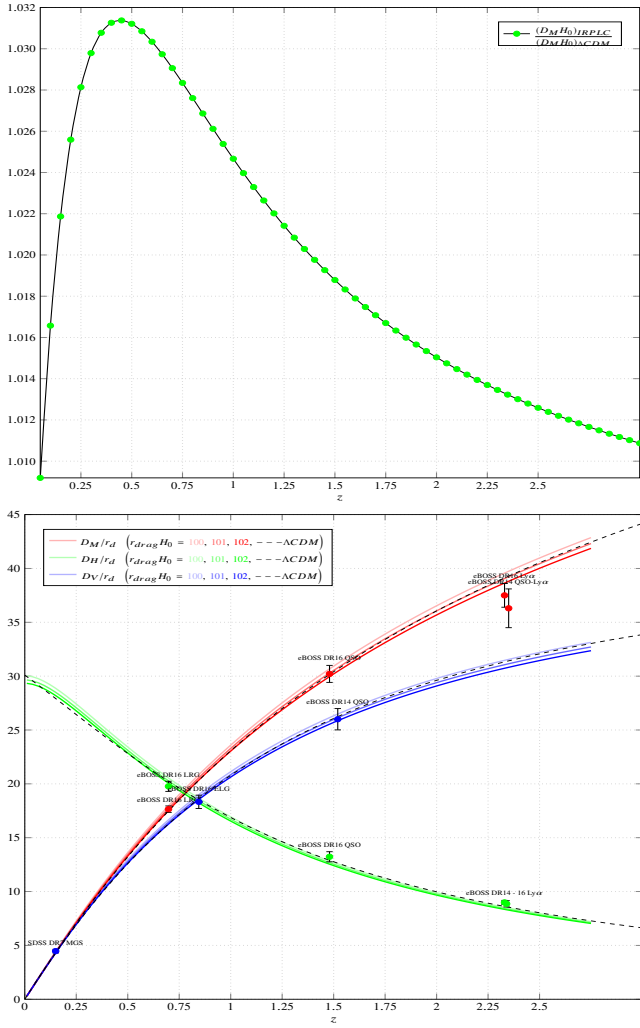
Figure 6. The top panel shows the rate between the normalized comoving distance $D_M H_0$ of fiducial IRPLC model and that of fiducial ΛCDM model. The bottom panel shows BAO "Hubble diagram" . Black dashed lines represent the fiducial ΛCDM model, coloured solid lines represent the fiducial IRPLC model for $H_0 r_{drag} = 100, 101, 102$.

and z_{drag} (table A1), making sure to use the appropriate values of $\omega_b(z)$ and $\omega_c(z)$ present at the redshift of interest, instead of the fitting formulas (Hu & Sugiyama 1996). For the same reason, the exact formula of the acoustic wave speed (74) was used, which also takes into account the pressure of matter, and not the approximate one, although the results differ by only a few units on the second decimal place.

Therefore, given the $IRPLC$ metric $\mathcal{M}_{IRPLC}(h)$ and the acoustic sound speed formula $c_s(\omega_b)$, for each ω_b we look for the value of h which satisfies both of the following equations at the same time:

$$z^* = z^*_{Camb}\left(\omega_{bs}(z^*), \omega_{cs}(z^*)\right) \tag{89}$$

$$\frac{r_s(z^*)}{\theta_* = 0.0104109} = d_M(z^*) \tag{90}$$

As a result, reaching an approximation of at most a few units on the second decimal place, we find that the acoustic angular scale constraint is satisfied by the values of z and h in accordance with the following fitting formulas in the range $H_0 = 73.48 \pm 1.5$ and

$$\Omega_b h^2 = 0.02325 \pm 0.005 \ (N_{eff} = 3.044) \ (\text{fig. } 8, 9)$$

$$z^* = 1134.3 + (H_0 - 73.48)\, 8.85 - 2000\left(\Omega_b h^2 - 0.02325\right) \pm 0.05 \tag{91}$$

$$H_0 = 73.48 \left(\frac{\omega_{0b}}{0.02325}\right)^{-0.0378} \pm 0.05 \quad Mpc^{-1}Km/sec \tag{92}$$

Likewise, taking into account the BAO measurements constraint:

$$z_{drag} = z_{drag_{Camb}}\left(\omega_{bs}(z_{drag}), \omega_{cs}(z_{drag})\right) \tag{93}$$

$$r_s(z_{drag})h \simeq 101 \pm 1 \tag{94}$$

we find the following additional limitations on the ω_{0b} and H_0 parameters (table A1 and fig. 6, 11, 8, 9):

$$r_{drag} \simeq \frac{101.052}{h}\left(\frac{\omega_{b_0}}{0.02325}\right)^{-0.0675} \pm 0.05 \quad Mpc \tag{95}$$

$$\omega_{b_0} = 0.02335 \pm 0.00335 \qquad H_0 = 73.5 \mp 0.4 \tag{96}$$

Remarkably, throughout the aforementioned wide range $\Omega_b h^2 = 0.02325 \pm 0.005$, the IRPLC metric together with the acoustic sound speed, having as the only free parameter to be able to vary the Hubble constant H_0, satisfy simultaneously all the first three aforementioned constraints. In particular, they satisfy the (89) and (90) with an accuracy of at most a few units on the second decimal place.

Regarding the baryon density limitation based on CMB constraints, found for the ΛCDM model, the same result can be applied equally well to the IRPLC model taking into account the appropriate causal region:

$$\omega_b(\theta^*) = \frac{\Omega_{b_0}}{(1 + \sin\theta^* + \theta^* \cos\theta^*)^2} = 0.02237 \pm 0.00015 \tag{97}$$

which gives $\Omega_{b_0} = 0.023311 \pm 0.000156$. Therefore

$$z^*(\Omega_{b_0}) = 1134.22 \mp 0.6 \qquad H_0(\Omega_{b_0}) = 73.47 \mp 0.03 \tag{98}$$

$$\omega_c(\gamma^*) = \frac{\omega_{c_0}}{(1 + \sin\gamma^* + \gamma^* \cos\gamma^*)^2} = 0.1213 \mp 0.0001 \tag{99}$$

At last, it is possible to use Camb software (fig. 10 and table A2), to get a first approximation of the temperature variations of the CMB within the IRPLC model. In the plot of fig. 10 we can see the Camb output, where the abscissas are slightly enlarged due to the slower velocity of c_s in the ΛCDM model .

Compared to the ΛCDM model, the IRPLC model solves the Hubble Tension (at 5σ) while having one less parameter to play with. It may also solve the lensing amplitude A_L tension (at more than 2σ) and the S_8 tension with cosmic shear data (at 3.2σ). A software system dedicated to IRPLC can check if this promise is kept.

BBN is one of the pillars of ΛCDM cosmology. The predictions of the standard BBN theory rest on balance between expansion rate and on the astrophysical nuclear reaction rates and on three additional parameters, the number of light neutrino flavours (N_ν), the neutron lifetime (τ_n) and the baryon-to-photon ratio ($\eta = n_B/n_\gamma$) in the universe (Copi et al. 1995). Compared to the ΛCDM model, with the same baryon-to-photon ratio ($\eta = n_B/n_\gamma$), in the IRPLC model the element densities during the BBN are half, and therefore the rates of astrophysical nuclear reactions during the BBN must be halved in the same way.

Table 1 and fig. 7 compare the values calculated by the IRPLC model with those of the ΛCDM model and with those measured. Both the abundances of lithium-7 and helium-4 are congruent

with the measured values. About the primordial ^{3}He abundance, at present there are no reliable measurements Cooke et al. (2018), since ^{3}He can be both created and destroyed in stars. At last, IRPLC BBN (table 1, table A3 and fig. 7) solves the lithium problem but, in its place, raises a deuterium problem.

About the acceleration in the expansion of the universe, being $d\tau = ad'_M(\gamma)d\gamma$ and $da = -\cos\gamma d\gamma$, we have :

$$\rho = \rho_r + \rho_m + \rho_s \tag{100}$$

$$3p/c^2 = \rho_r + \rho_m - \rho_s - 2\cos\gamma \frac{d''_{M_m}(\gamma)}{d'_{M_m}(\gamma)}\rho_m \tag{101}$$

$$\dot{a} = -\frac{\cos\gamma}{ad'_M(\gamma)} \tag{102}$$

$$\ddot{a} = \frac{-1}{a^2 d'^2_M(\gamma)} + \cos\gamma \frac{d''_M(\gamma)}{d'_M(\gamma)} \frac{1}{a^2 d'^2_M(\gamma)} \tag{103}$$

and therefore we find

$$\frac{2}{H_0^2}\frac{\ddot{a}}{a} = \frac{-1}{\rho_{crit}}\left(\rho + 3p/c^2\right)$$

as required by the Friedmann's second equation (5).

From the (101, 103), it follows that the accelerated expansion of the universe (fig. 12) has begun since $z \simeq 0.5099$ when the universe was 7.996 billion years old, roughly almost 5 billion years ago, since the age of the universe is 12.826 billion years.

5 GALAXY ROTATION CURVES

Contrary to what happens in cosmology, where $r \leq R_\Omega$, the gravitational motion of galaxies [5] takes place outside its own Schwarzschild Radius ($r \geq R_{galaxy}$). The gravitational radius of a galaxy, neglecting the radiation, and since, from the (eq.43), $R_c \simeq r^2/R_0$, is :

$$R = \Omega_b R + \Omega_r R + \Omega_c R = R_b + R_c + R_r \simeq R_b + r^2/R_0 + 0 \tag{104}$$

Similarly to what has been done in cosmology, it is possible to decompose the distance according to the type of energy and in particular it is convenient to impose that the curvature radius, equal to the inverse of the acceleration, is the same for all the components everywhere, namely:

$$A_x = \frac{R_x}{r_x^2} = A = \frac{R}{r^2} = \frac{1}{\tau^\diamond} \qquad (R_{galaxy} \leq \tau^\diamond \leq R_0) \tag{105}$$

which is the dual of the (43) for $r \geq R$. This condition is satisfied by $r_x = \sqrt{\Omega_x}\, r$ or, equivalently:

$$r^2 = r_b^2 + r_r^2 + r_c^2 = \Omega_b r^2 + \Omega_r r^2 + \Omega_c r^2 \tag{106}$$

which is the dual of the (52) for $r \geq R$ (note that, since $R \simeq R_b + R_c$, we have $A_{gravitational} \simeq \frac{R_b}{r^2} + \frac{1}{R_0}$).

If we set

$$A_{centrifugal} = \frac{v_{centrifugal}^2}{r_b} \tag{107}$$

---
[5] the b_Γ factor $1 + \sin\Gamma_{DIM_{galaxy}} \leq 1 + \sin\Gamma_{100\,kpc} \leq 1 + 10^{-5}$ is negligible.

since in the orbital motion $A_{gravitational} = A_{centrifugal}$, it follows:

$$v_{centrifugal} = \sqrt{V_b} = \sqrt[4]{\frac{R}{r^2}R_b} = \sqrt[4]{\frac{R_b^2}{r^2} + \frac{R_b}{R_0}} \tag{108}$$

and the limits

$$r_{b_\infty} = \lim_{r \to R_0} \sqrt{\frac{R_b}{R}}r = \sqrt{R_b R_0} \tag{109}$$

$$v_\infty = \lim_{r \to R_0} \sqrt[4]{\frac{R_b^2}{r^2} + \frac{R_b}{R_0}} = \sqrt[4]{\frac{R_b}{R_0}} \tag{110}$$

On circular orbit, where $R_0 = 2\pi c H_0^{-1}$, we find (see fig. 13), with the same mass distribution, that the predictions for the galaxy rotation curves from present work (eq. 108) and MSTG and Milgrom's Mond agree remarkably for all of the 101 galaxies reported in (Brownstein & Moffat 2006). It is relevant that the Newton velocity, once replaced the total distance r with the distance r_b, is consistent with the experimented values everywhere (see fig. 13).

On radial orbits, stars plunging in and out of the galactic center, $R_0 = cH_0^{-1}$, as in motion of satellite galaxies around normal galaxies at distances 50-500 kpc (Klypin & Prada 2009), the rotation curves are considerably affected by the radial component of the motion which gradually decreases as moving away from the host galaxy. The maximum speed $v_\infty = \sqrt[4]{\frac{R_b}{R_0}}$ consequently decreases as $\sqrt[-4]{2\pi}$ as the initial radial speed turns into tangential speed moving away from the host galaxy consistently with the experimental results.

6 CONCLUSION

Surprisingly, the BBN theory of the IRPLC, which predicts the halving of the rates of primordial nuclear reactions compared to the standard model theory, is supported by measurements of primordial element abundances at least as much as the latter, while predicting very different results. It is still absolutely remarkable that the IRPLC model satisfies the cosmological constraints deriving from the CMB and BAO and from the acceleration of the expansion of the universe, while being able to count on one less parameter, in an equally satisfactory way compared to the ΛCDM model. Mostly, it solves the tension between the direct and the inverse cosmic distance ladder. At last, the model is successful on both large and small scales by solving, with the same hypothesis underlying the IRPLC model, the difficulties related to rotation in the inner parts of spiral galaxies with results similar to that of the Mond theory.

About the matter density, it does not violate the cosmological principle of the homogeneity of space because it applies equally in every place. Furthermore, its dependence on distance implies that the dimensions of the CDM correspond to the quantum of space, thus, it is to be expected that it will never be observed directly. More precisely, if ordinary matter is matter in act, CDM is matter in potency.

In summary, the following points apply to the universe:

• the universe has a curvature radius R_0 equal to its gravitational radius R_Ω

• the horizon of the present in act has constant surface gravity equal to H_0

• the change of energy ($r_s = r^2/R_0$ from hypothesis 1) is related

[h!]

Table 1. Primordial abundances of elements in the big-bang nucleosynthesis (BBN)
For the measured values see: (a) Aver et al. (2021), (b) Cooke et al. (2018) , (c) Bania et al. (2002), (d) Sbordone et al. (2010)
For the ΛCDM calculated values see: Pitrou et al. (2021)
The IRPLC calculated values were produced by the software AlterBBN halving all the rates of nuclear reactions and with $\eta = 6.38158 \times 10^{-10}$, $\tau_n = 879.4$, $N_{eff} = 3.044$

	Yp (10^{-01})	D/H (10^{-05})	^{3}He/H (10^{-05})	^{7}Li/H (10^{-10})
Observations:	2.453 ± 0.034 (a)	2.527 ± 0.030 (b)	1.1 ± 0.2 (c)	$1.58 ^{+0.35}_{-0.28}$ (d)
ΛCDM ($\eta_{10} = 6.13792$):	2.4721 ± 0.00014	2.439 ± 0.037	1.039 ± 0.014	**5.464 ± 0.220**
IRPLC ($\eta_{10} = 6.38158$):	2.447 ± 0.0032	**6.528 ± 0.063**	1.502 ± 0.016	1.568 ± 0.11

[h!]

Table 2. Parameters for the base ΛCDM and IRPLC models compared
Comparison between IRPLC parameters and Parameter 68% intervals for the base-ΛCDM model from Planck CMB power spectra, in combination with CMB lensing reconstruction (Planck Collaboration et al. 2020).

Parameter	ΛCDM TT,TE,EE+LowE+lensing 68% limits	IRPLC	IRPLC special cases
$\omega_{0_b} h^2$	0.02237 ± 0.00015	0.02325 ∓ 0.00035	$\omega_b(\theta^*) = 0.02231 \mp 0.00033$
$\omega_{0_c} h^2$	0.1200 ± 0.0012	0.5166 ± 0.001	$\omega_c(z^*) = 0.1213 \pm 0.0002$
$100\theta_{MC}$	1.04092 ± 0.00031	idem	
τ	0.0544 ± 0.0073	idem	
$ln\left(10^{10} A_s\right)$ . . .	3.044 ± 0.014	idem	
n_s	0.9649 ± 0.0042	idem	
$H_0 [kms^{-1}Mpc^{-1}]$	67.36 ± 0.54	73.48 ± 0.04	
Ω_Λ	0.6847 ± 0.0073		
Ω_m	0.3153 ± 0.0073	$0.999923 \pm 8 \times 10^{-8}$	
Age[Gyr]	13.797 ± 0.023	12.815 ∓ 0.07	
z^*	1089.92 ± 0.25	1134.3 ± 0.05	
$r^* [Mpc]$	144.43 ± 0.26	129.44 ∓ 0.05	
$100\theta^*$	1.04110 ± 0.00031	1.04101	
z_{drag}	1059.94 ± 0.30	1036.45 ∓ 0.7	
$r_{drag} [Mpc]$ . .	147.09 ± 0.26	137.52 ± 0.7	
z_{eq}	3402 ± 26	$z_{eq_{ms}} = 6286.95 \pm 8.6$	$z_{eq_m} = 3108.37 \pm 4.3$

to change of area A, angular momentum J, and electric charge Q by

$$dE = \frac{\kappa}{8\pi} dA + \Omega\, dJ + \Phi\, dQ \tag{111}$$

for $dJ = dQ = 0$, being the surface gravity $\kappa = 1/r$ and where A is the horizon area.

At last, these evidences suggest an alternative solution to the causal horizon problem. In fact, the ad hoc hypothesis of inflation could be replaced by the following more natural and general hypothesis:

Hypothesis 2 *The universe is a white/black hole with constant Schwarzschild Radius $R_\Omega \equiv c/H_0$ where the big bang/big crunch is not an event of the past but a continuous feedback process, always in progress, typical of all black holes. It follows that the surface of the present in act ($\gamma = 0$), as well as the big bang in act ($\gamma \pm \pi/2$), are the frontiers where the approaching future becomes present and is converted in the past that moves away and vice versa, in an eternal cycle.*

To every observer, on the present in act (which is a special place), the universe appears to have two special places: the big bang in act and the big crunch in act. They are dual and symmetrical: each of the two is the horizon of the present in act and vice versa; both, as well as the present in act, are on the surface of the hypersphere which is the Universe.

In other words, the internal volume of the sphere is the seat of potency while the surface is the place of the present in act where the temporal axis of each individual emerges radially dividing the surface of the black hole into its own receiving hemisphere ($0 \geq \gamma \leq \pi/2$), populated by all other individuals in the act of giving as matter, where the arrow of time is positive and entropy increases, and in its opposite giving hemisphere ($\pi/2 \geq \gamma \leq \pi$), populated by individuals in the act of receiving as antimatter, where the arrow of time is negative and entropy decreases. In other words, for each individual, the present, which comes from the continuous Big Bang (as source) as an approaching future (matter and increasing entropy), as soon as it surfaces, it submerge as past (antimatter and decreasing entropy) that move away to go towards the continuous Big Crunch (as well), and in this descent informs of itself the future that ascend in the opposite direction. The past that is moving away is also the future that is approaching, and it is the possibility of the present. The present is the realization of a possible history of the past, among the totality of physically possible histories in accordance with quantum mechanics.

The mechanism that places the same initial conditions everywhere, therefore, is not to be found in a causal contact occurred in the past of a linear time, but in the dialogue, with a period P_ω equal to the apparent age of the universe, between the big bang and the present, in a cyclical time: each time, the new present in act is the result of the big bang that took place P_ω years before and is the foundation of the big bang that will take place P_ω years later.
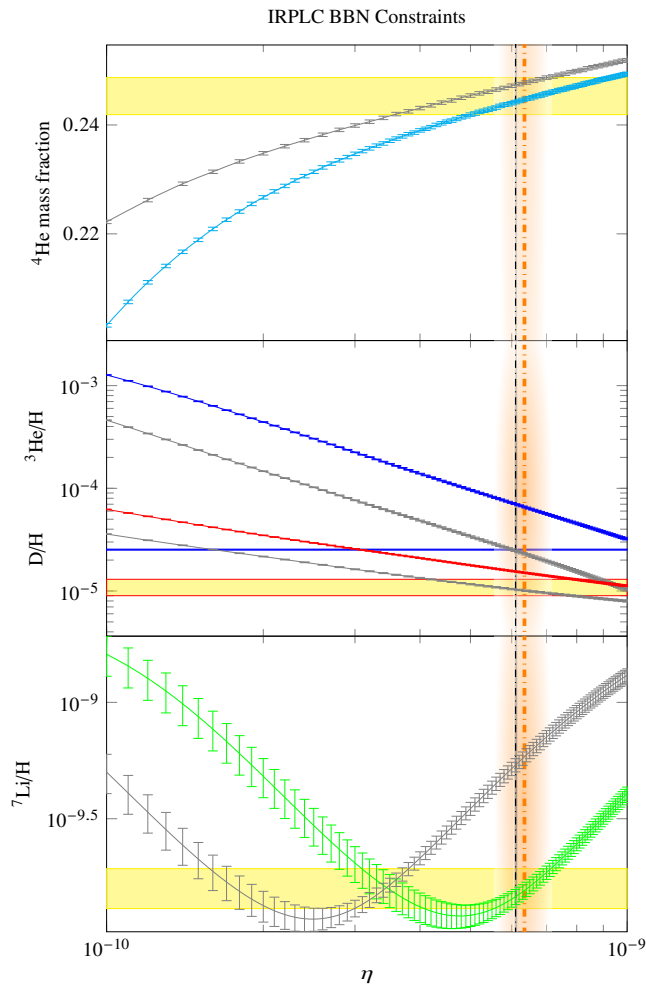
Figure 7. Comparison between the primordial abundances expected for the light nuclei according to the ΛCDM model, grey lines, and the IRPLC model, coloured lines. Yellow horizontal rectangles show range of the uncertainties in the primordial abundances measured values (see table A3). The orange vertical line indicates the value of $\eta = 6.35 \pm 0.8 \times 10^{-10}$ deduced in the present IRPLC analysis, the grey one $\eta = 6.105 \pm 0.055 \times 10^{-10}$ for the ΛCDM model (Mindari et al. 2018). The values were calculated using the version 2 of *AlterBBN* software, an open public code for the calculation of the abundance of the elements from Big-Bang nucleosynthesis. For the purpose of the IRPLC model, the *bbnrate.c* file was modified by adding the instruction " **f[ie]=0.5*f[ie];** " at the end of the loop of the *rate all* function in order to halve all the reaction rates.

This hypothesis, compared to the correspondent of standard cosmology, radically changes the meaning but leaves the entire phenomenology and physics of the universe unchanged.

If this hypothesis is correct, all the parameters of the universe, such as the temperature of the CMB or Ω_b, Ω_c, Ω_r etc., are not contingent.

7 DATA AVAILABILITY STATEMENT

The data underlying this article are available in the article and in its online supplementary material.
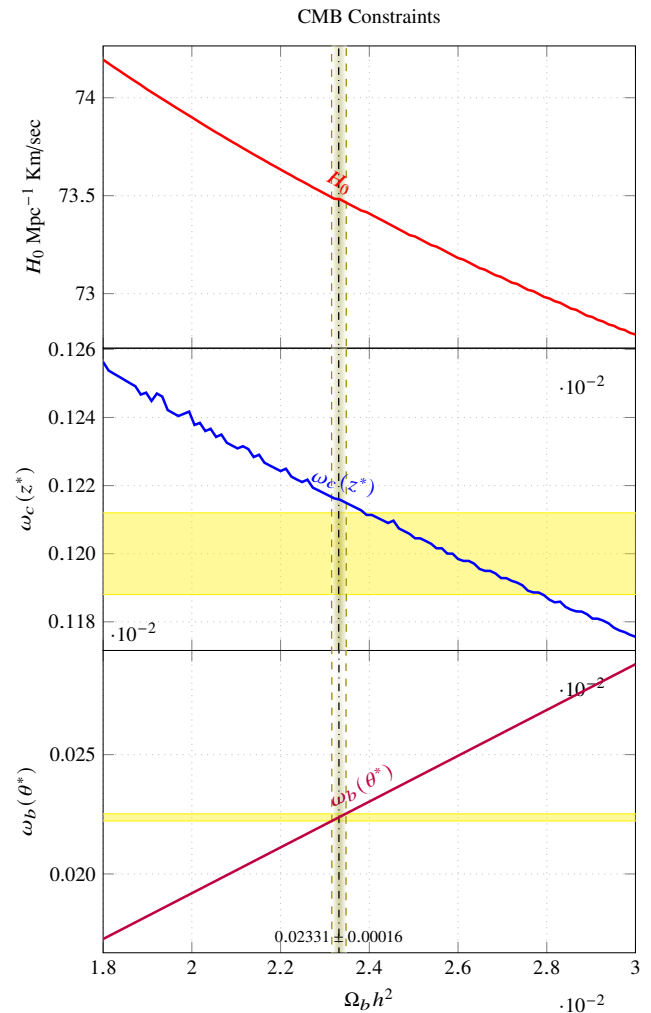
Figure 8. The CMB constraints on the Hubble constant.

REFERENCES

Addison G. E., Huang Y., Watts D. J., Bennett C. L., Halpern M., Hinshaw G., Weiland J. L., 2016, ApJ, 818, 132

Akita K., Yamaguchi M., 2020, J. Cosmology Astropart. Phys., 2020, 012

Aubourg A., Balembois F., Georges P., 2014, Laser Physics Letters, 11, 048001

Aver E., Berg D. A., Olive K. A., Pogge R. W., Salzer J. J., Skillman E. D., 2021, J. Cosmology Astropart. Phys., 2021, 027

Bania T. M., Rood R. T., Balser D. S., 2002, Nature, 415, 54

Bennett J. J., Buldgen G., Drewes M., Wong Y. Y. Y., 2020, J. Cosmology Astropart. Phys., 2020, 003

Brownstein J. R., Moffat J. W., 2006, ApJ, 636, 721

Cooke R. J., Pettini M., Steidel C. C., 2018, ApJ, 855, 102

Copi C. J., Schramm D. N., Turner M. S., 1995, Science, 267, 192

Di Valentino E., et al., 2021, Classical and Quantum Gravity, 38, 153001

Einstein A., 1905, Annalen der Physik, 322, 891

Einstein A., 1923, The Meaning of Relativity, 1 edn. Princeton University Press, Princeton, NewJersey

Escudero Abenza M., 2020, J. Cosmology Astropart. Phys., 2020, 048

Feynman R. P., 1985, QED: The Strange Theory of Light and Matter, 1 edn. Princeton University Press, Princeton, NewJersey

Fixsen D. J., 2009, ApJ, 707, 916

Froustey J., Pitrou C., Volpe M. C., 2020, J. Cosmology Astropart. Phys., 2020, 015
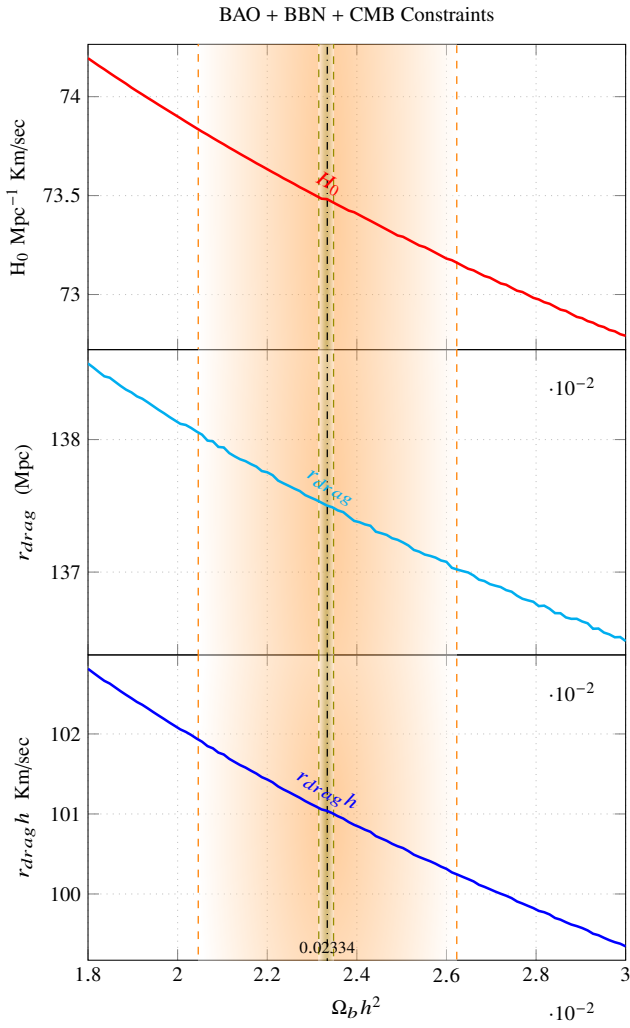
Figure 9. The superimposition of all the constraints on the parameters of the IRPLC model.
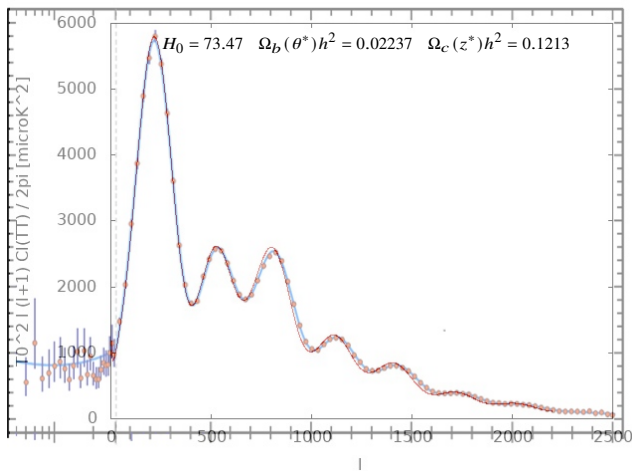
Figure 10. The CMB temperature (E-mode polarization), output of CAMB with $\Omega_c(z^*)h^2 = 0.1213$, $\Omega_b(\theta^*)h^2 = 0.02237$ (which corresponds to $\Omega_{0_b}h^2 = 0.02331$).
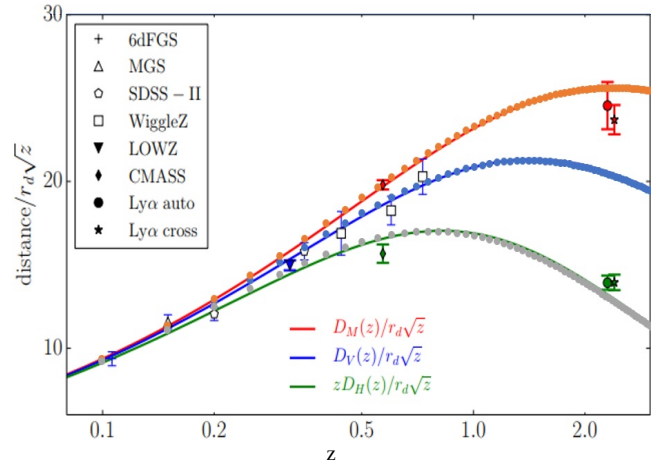
Figure 11. The BAO "Hubble diagram" (from Aubourg et al. 2014). Blue, red, and green points show BAO measurements of d_V/r_d, d_M/r_d, and zd_H/r_d, respectively, from the sources indicated in the legend. The scaling by $\sqrt{z}$ is arbitrary, chosen to compress the dynamic range sufficiently to make error bars visible on the plot. These can be compared to the correspondingly colored lines, which represents predictions of the fiducial Planck ΛCDM model (with $m = 0.3183$, $h = 0.6704$) and the prediction of the IR-PLC model (dotted line) when $r_{s_{drag}} = 101.0/h$ Mpc.

Grohs E., Fuller G. M., 2017, Nuclear Physics B, 923, 222
Hu W., Dodelson S., 2002, ARA&A, 40, 171
Hu W., Sugiyama N., 1996, ApJ, 471, 542
Klypin A., Prada F., 2009, ApJ, 690, 1488
Landau L. D., Lifshitz E. M., 1971, The Classical Theory of Fields, 3 edn. Pergamon Press Ltd., Headington Hill Hall, Oxford
Mangano G., Miele G., Pastor S., Pinto T., Pisanti O., Serpico P. D., 2005, Nuclear Physics B, 729, 221
Mindari W., Sasongko P. E., Kusuma Z., Syekhfani Aini N., 2018, in The 9th International Conference on Global ReSource Conservation (ICGRC) and Aji from Ritsumeikan University. p. 030001, doi:10.1063/1.5061854
Peluso V. 13 jan 2019 viXra, viXra:1811.0391
Peluso V. 25 sep 2019 viXra, viXra:1909.0552
Peluso V. 19 jun 2020 viXra, viXra:2003.0606
Peluso V. 16 apr 2021 viXra, viXra:2104.0097
Pitrou C., Coc A., Uzan J.-P., Vangioni E., 2021, MNRAS, 502, 2474
Planck Collaboration et al., 2020, A&A, 641, A6
Reid M. J., Pesce D. W., Riess A. G., 2019, ApJ, 886, L27
Riess A. G., et al., 1998, AJ, 116, 1009
Riess A. G., et al., 2021, arXiv e-prints, p. arXiv:2112.04510
Sbordone L., et al., 2010, A&A, 522, A26
Vonlanthen M., Räsänen S., Durrer R., 2010, J. Cosmology Astropart. Phys., 2010, 023
Wong K. C., et al., 2020, Monthly Notices of the Royal Astronomical Society, 498, 1420
de Salas P. F., Pastor S., 2016, J. Cosmology Astropart. Phys., 2016, 051

Acceleration of the expansion of the universe

Rotation curve for the elliptical galaxy NGC 3379
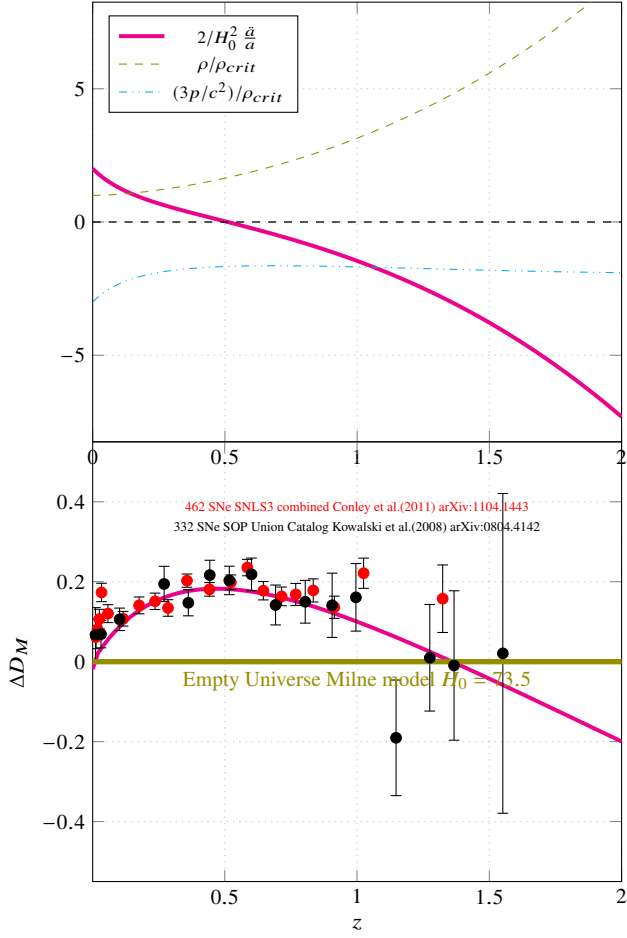
Figure 12. The top panel shows the pressure $3p/c^2 = \rho_r + \rho_m - \rho_s - 2\cos\gamma \frac{d_M''(\gamma)}{d_M'(\gamma)}\rho_m$, the density $\rho = \rho_r + \rho_m + \rho_s$ and the acceleration $\frac{2}{H_0^2}\frac{\ddot{a}}{a} = \frac{-1}{\rho_{crit}}\left(\rho + 3p/c^2\right)$ in the expansion of the universe.

On the bottom panel, the brightness or faintness of distant supernovae relative to the empty Universe model $\Omega = 0$ (the green curve) is plotted vs redshift.

The blue-red curve, $\Delta(d_M) = 5\log_{10}\left(\frac{d_L}{R_\omega z\left(1+\frac{z}{2}\right)}\right)$ is the difference between

the distance modulus determined from the computed flux $d_L = d_M(1+z)$ and the distance modulus computed from the redshift in the empty Universe model. The Hubble constant used in computing the empty Universe Milne model which is subtracted off is 73.5 km/sec/Mpc, and not 63.8 as in Riess et al. (2007).
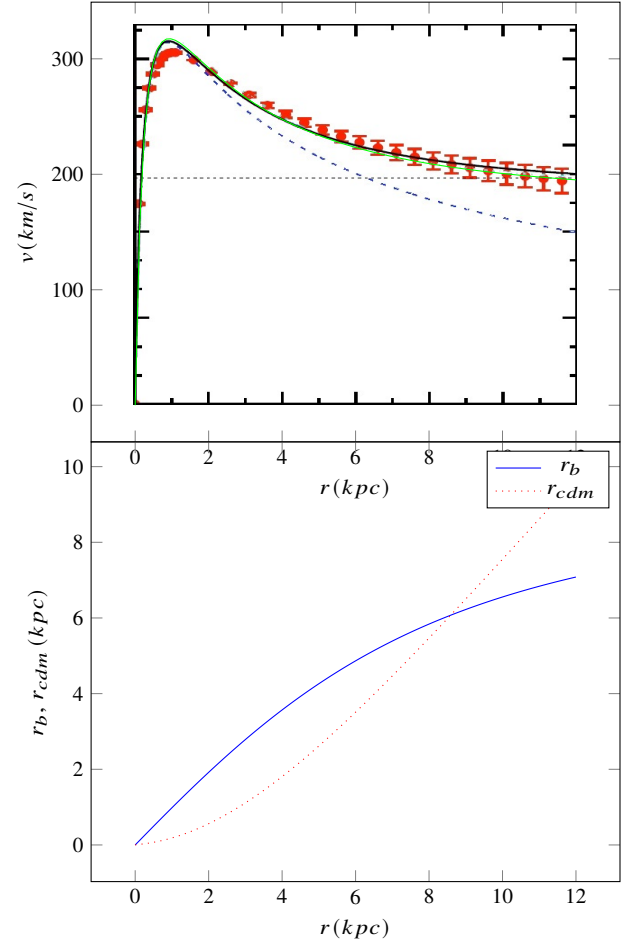
Figure 13. On the top panel, the rotation curve for the elliptical galaxy NGC 3379. The red points (with error bars) are the observations. The solid green line is the rotation curve determined by the present work (eq. 108), the short dashed blue line is the Newtonian galaxy rotation curve. The same distribution of the galactic mass reported in (Brownstein & Moffat 2006) has been adopted, that is $M = 6.99\,10^{10}\,M_\odot$, and a core radius $r_c = 0.45$ kpc and $\beta = 1$.

On the bottom panel, the trend of r_b and r_{cdm}. The rotation curve also corresponds to Newton's velocity once replaced the total distance r with the distance r_b.

APPENDIX A: IRPLC PARAMETER TABLES

This paper has been typeset from a T$_{\text{E}}$X/L$^{\text{A}}$T$_{\text{E}}$X file prepared by the author.

[H]

Table A1. IRPLC parameters that satisfy the constraints 1,2,3
the table shows, as the baryon density varies, the values assumed by the parameters of the IRPLC model that satisfy the first five constraints. It should be noted that the redshift z^* that satisfies the constraint of the acoustic angular scale coincides with that calculated by CAMB based on the baryon and CDM densities at z^*

	IRPLC values satisfying constraints 1,2,3					CAMB input		output	CAMB input		output
ω_{0_b}	H_0	z^*	r^*	z_d	r_{drag}	$\omega_{bs}(z^*)$	$\omega_{cs}(z^*)$	z^*	$\omega_{bs}(z_d)$	$\omega_{cs}(z_d)$	z_d
. . .	. . .	. . .	. . .	. . .	. . .	. . .	. . .	. . .	. . .	. . .	. . .
0.022	73.63	1138.15		1034.0		0.010332	0.244284	1138.03	0.010302	0.243574	1034.03
0.02205	73.63	1138.00		1034.1		0.010355	0.244216	1137.88	0.010325	0.243508	1034.12
0.0221	73.62	1137.84		1034.2		0.010379	0.244148	1137.73	0.010348	0.243441	1034.22
0.02215	73.61	1137.69		1034.3		0.010402	0.244080	1137.58	0.010372	0.243375	1034.32
0.0222	73.61	1137.53		1034.4		0.010425	0.244012	1137.43	0.010395	0.243309	1034.42
0.02225	73.60	1137.38		1034.5		0.010449	0.243945	1137.28	0.010419	0.243243	1034.51
0.0223	73.60	1137.22		1034.6		0.010472	0.243877	1137.13	0.010442	0.243178	1034.61
0.02235	73.59	1137.07		1034.7		0.010496	0.243809	1136.98	0.010466	0.243112	1034.71
0.0224	73.58	1136.91		1034.8		0.010519	0.243742	1136.83	0.010489	0.243047	1034.80
0.02245	73.58	1136.76		1034.9		0.010543	0.243675	1136.68	0.010513	0.242981	1034.90
0.0225	73.56	1136.51	129.3	1035.2	137.67	0.010566	0.243534	1136.51	0.010536	0.242844	1035.27
0.02255	73.56	1136.45		1035.0		0.010589	0.243541	1136.39	0.010559	0.242850	1035.09
0.0226	73.56	1136.29		1035.1		0.010613	0.243474	1136.24	0.010583	0.242785	1035.19
0.02265	73.55	1136.14		1035.2		0.010636	0.243407	1136.09	0.010606	0.242720	1035.28
0.0227	73.55	1135.98		1035.3		0.010660	0.243340	1135.94	0.010630	0.242655	1035.38
0.02275	73.54	1135.83		1035.4		0.010683	0.243273	1135.79	0.010653	0.242590	1035.48
0.0228	73.53	1135.68		1035.57		0.010707	0.243207	1135.64	0.010677	0.242526	1035.58
0.02285	73.53	1135.53		1035.67		0.010731	0.243141	1135.49	0.010701	0.242462	1035.67
0.0229	73.52	1135.37		1035.76		0.010754	0.243074	1135.35	0.010724	0.242397	1035.77
0.02295	73.52	1135.22		1035.86		0.010778	0.243008	1135.2	0.010748	0.242333	1035.86
0.023	73.51	1135.07		1035.95		0.010801	0.242942	1135.05	0.010771	0.242268	1035.95
0.02305	73.5	1134.91		1036.05		0.010824	0.242876	1134.9	0.010794	0.242204	1036.05
0.0231	73.5	1134.76		1036.14		0.010848	0.242810	1134.75	0.010818	0.242140	1036.14
0.02315	73.49	1134.61		1036.24		0.010871	0.242744	1134.6	0.010841	0.242076	1036.24
0.0232	73.49	1134.45		1036.33		0.010895	0.242678	1134.45	0.010865	0.242012	1036.33
0.02325	73.48	1134.3	129.44	1036.43	137.52	0.010918	0.242612	1134.3	0.010888	0.241948	1036.42
0.0233	73.47	1134.15		1036.52		0.010942	0.242547	1134.15	0.010912	0.241884	1036.52
0.02335	73.47	1133.99		1036.61		0.010965	0.242481	1134	0.010935	0.241820	1036.61
0.0234	73.46	1133.84		1036.71		0.010988	0.242416	1133.85	0.010959	0.241757	1036.71
0.02345	73.46	1133.69		1036.8		0.011012	0.242350	1133.7	0.010982	0.241693	1036.8
0.0235	73.45	1133.54		1036.89		0.011035	0.242285	1133.55	0.011005	0.241630	1036.89
0.02355	73.44	1133.38		1036.99		0.011059	0.242220	1133.4	0.011029	0.241566	1036.99
0.0236	73.44	1133.23		1037.08		0.011082	0.242155	1133.25	0.011052	0.241503	1037.08
0.02365	73.43	1133.08		1037.17		0.011106	0.242090	1133.11	0.011076	0.241440	1037.17
0.0237	73.43	1132.93		1037.26		0.011129	0.242025	1132.96	0.011099	0.241377	1037.26
0.02375	73.42	1132.78		1037.36		0.011152	0.241960	1132.81	0.011123	0.241314	1037.36
0.0238	73.42	1132.63		1037.45		0.011176	0.241896	1132.66	0.011146	0.241251	1037.45
0.02385	73.41	1132.47		1037.54		0.011199	0.241831	1132.51	0.011170	0.241188	1037.54
0.0239	73.4	1132.32		1037.63		0.011223	0.241767	1132.36	0.011193	0.241126	1037.63
0.02395	73.4	1132.17		1037.72		0.011246	0.241702	1132.21	0.011216	0.241063	1037.72
0.024	73.39	1132.02		1037.82		0.011270	0.241638	1132.06	0.011240	0.241000	1037.81
0.02405	73.39	1131.87		1037.91		0.011293	0.241574	1131.91	0.011263	0.240938	1037.91
0.0241	73.38	1131.72		1038		0.011317	0.241510	1131.76	0.011287	0.240876	1038
0.02415	73.37	1131.57		1038.09		0.011340	0.241446	1131.61	0.011310	0.240813	1038.09
0.0242	73.37	1131.42		1038.18		0.011363	0.241382	1131.46	0.011334	0.240751	1038.18
. . .	. . .	. . .	. . .	. . .	. . .	. . .	. . .	. . .	. . .	. . .	. . .

[H]

Table A2. (Vonlanthen et al. 2010) find that every model which satisfies $100\omega_b = 2.13 \pm 0.05$, $\omega_c = 0.124 \pm 0.007$, $n_s = 0.93 \pm 0.02$, $\theta^* = 0.593° \pm 0.001°$ will automatically be in agreement with the CMB data for $\ell \geq 40$. Only lower ℓ CMB data, large scale structure, lensing and other observations can distinguish between models which have the above values for ω_b, ω_c, n_s and θ^*

| ω_{0_b} | η | z^* | H_0 | CAMB input parameters for TT, TE and EE power spectra | | | | |
				$\omega_b\,(\theta^* = 0.0104109)$	$\omega_b\,(z^*)$	$\omega_c\,(z^*)$	$\omega_m\,(z^*)$	He/H
$\cdots$	$\cdots$	$\cdots$	$\cdots$	$\cdots$	$\cdots$	$\cdots$	$\cdots$	$\cdots$
0.02195	6.00925×10^{-10}	1138.3	73.63	0.02106	0.00516	0.12221	0.12737	
0.022	6.02294×10^{-10}	1138.1	73.63	0.02111	0.00517	0.122175	0.12734	
0.02205	6.03663×10^{-10}	1138.0	73.62	0.02116	0.00518	0.122141	0.12732	
0.0221	6.05032×10^{-10}	1137.8	73.62	0.02121	0.00519	0.122107	0.1273	
0.02215	6.06401×10^{-10}	1137.6	73.61	0.02126	0.00520	0.122073	0.12728	
0.0222	6.07769×10^{-10}	1137.5	73.6	0.0213	0.00522	0.122039	0.12725	
0.02225	6.09138×10^{-10}	1137.3	73.6	0.02135	0.00523	0.122006	0.12723	0,2442
0.0223	6.10507×10^{-10}	1137.2	73.59	0.0214	0.00524	0.121972	0.12721	
0.02235	6.11876×10^{-10}	1137.0	73.58	0.02145	0.00525	0.121938	0.12719	
0.0224	6.13245×10^{-10}	1136.9	73.58	0.0215	0.00526	0.121904	0.12717	
0.02245	6.14614×10^{-10}	1136.6	73.56	0.02154	0.00527	0.121833	0.12711	
0.0225	6.15983×10^{-10}	1136.6	73.57	0.02159	0.00529	0.121837	0.12712	
0.02255	6.17351×10^{-10}	1136.4	73.56	0.02164	0.00530	0.121803	0.1271	
0.0226	6.18720×10^{-10}	1136.2	73.55	0.02169	0.00531	0.12177	0.12708	0,2444
0.02265	6.20089×10^{-10}	1136.1	73.55	0.02174	0.00532	0.121736	0.12706	
0.0227	6.21458×10^{-10}	1135.9	73.54	0.02178	0.00533	0.121703	0.12704	
0.02275	6.22827×10^{-10}	1135.8	73.53	0.02183	0.00534	0.12167	0.12701	
0.0228	6.24196×10^{-10}	1135.6	73.53	0.02188	0.00536	0.121636	0.12699	
0.02285	6.25564×10^{-10}	1135.5	73.52	0.02193	0.00537	0.121603	0.12697	
0.0229	6.26933×10^{-10}	1135.3	73.52	0.02198	0.00538	0.12157	0.12695	
0.02295	6.28302×10^{-10}	1135.2	73.51	0.02202	0.00539	0.121537	0.12693	
0.023	6.29671×10^{-10}	1135.0	73.5	0.02207	0.00540	0.121504	0.12691	0,2446
0.02305	6.31040×10^{-10}	1134.9	73.5	0.02212	0.00541	0.121471	0.12689	
0.0231	6.32409×10^{-10}	1134.7	73.49	0.02217	0.00543	0.121438	0.12686	
0.02315	6.33778×10^{-10}	1134.6	73.49	0.02222	0.00544	0.121405	0.12684	
0.0232	6.35146×10^{-10}	1134.4	73.48	0.02226	0.00545	0.121372	0.12682	
0.02325	6.36515×10^{-10}	1134.3	73.48	0.02231	0.00546	0.121342	0.1268	
0.0233	6.37884×10^{-10}	1134.1	73.47	0.02236	0.00547	0.121306	0.12678	
0.02335	6.39253×10^{-10}	1133.9	73.46	0.02241	0.00548	0.121273	0.12676	
0.0234	6.40622×10^{-10}	1133.8	73.46	0.02246	0.00550	0.12124	0.12674	0,2448
0.02345	6.41991×10^{-10}	1133.6	73.45	0.0225	0.00551	0.121208	0.12672	
0.0235	6.43360×10^{-10}	1133.5	73.44	0.02255	0.00552	0.121175	0.1267	
0.02355	6.44728×10^{-10}	1133.3	73.44	0.0226	0.00553	0.121143	0.12667	
0.0236	6.46097×10^{-10}	1133.2	73.43	0.02265	0.00554	0.12111	0.12665	
0.02365	6.47466×10^{-10}	1133.0	73.43	0.0227	0.00556	0.121078	0.12663	
0.0237	6.48835×10^{-10}	1132.9	73.42	0.02274	0.00557	0.121045	0.12661	
0.02375	6.50204×10^{-10}	1132.7	73.41	0.02279	0.00558	0.121013	0.12659	0,2449
0.0238	6.51573×10^{-10}	1132.6	73.41	0.02284	0.00559	0.12098	0.12657	
0.02385	6.52941×10^{-10}	1132.4	73.4	0.02289	0.00560	0.120948	0.12655	
0.0239	6.54310×10^{-10}	1132.3	73.4	0.02293	0.00561	0.120916	0.12653	
0.02395	6.55679×10^{-10}	1132.1	73.39	0.02298	0.00563	0.120884	0.12651	
0.024	6.57048×10^{-10}	1132.0	73.39	0.02303	0.00564	0.120851	0.12649	
0.02405	6.58417×10^{-10}	1131.8	73.38	0.02308	0.00565	0.120819	0.12647	
0.0241	6.59786×10^{-10}	1131.7	73.37	0.02313	0.00566	0.120787	0.12645	
0.02415	6.61155×10^{-10}	1131.5	73.37	0.02317	0.00567	0.120755	0.12643	0,2451
$\cdots$	$\cdots$	$\cdots$	$\cdots$	$\cdots$	$\cdots$	$\cdots$	$\cdots$	$\cdots$

[H]

Table A3. Primordial abundances of elements in the big-bang nucleosynthesis (BBN)

For the measured values see: (a) Aver et al. (2021), (b) Cooke et al. (2018) , (c) Bania et al. (2002), (d) Sbordone et al. (2010)

The calculated values were produced by the software AlterBBN halving all the rates of nuclear reactions and with $\eta = 6.36515 \times 10^{-10}$, $\tau_n = 879.4$, $N_{eff} = 3.044$

	Yp (10^{-01})	D/H (10^{-05})	^{3}He/H (10^{-05})	^{7}Li/H (10^{-10})
measured values:	2.453 ± 0.034 (a)	2.527 ± 0.030 (b)	1.1 ± 0.2 (c)	1.58 $^{+0.35}_{-0.28}$ (d)
...	...	...	...	...
calculated values ($\eta_{10} = 5.5$):	2.430 ± 0.0032	8.283 ± 0.074	1.666 ± 0.016	1.290 ± 0.11
calculated values ($\eta_{10} = 5.6$):	2.432 ± 0.0032	8.046 ± 0.072	1.645 ± 0.016	1.312 ± 0.11
calculated values ($\eta_{10} = 5.7$):	2.435 ± 0.0032	7.821 ± 0.071	1.624 ± 0.016	1.337 ± 0.11
calculated values ($\eta_{10} = 5.8$):	2.437 ± 0.0032	7.606 ± 0.069	1.605 ± 0.016	1.365 ± 0.11
calculated values ($\eta_{10} = 5.9$):	2.438 ± 0.0032	7.400 ± 0.068	1.586 ± 0.016	1.395 ± 0.11
calculated values ($\eta_{10} = 6.0$):	2.440 ± 0.0032	7.204 ± 0.067	1.567 ± 0.016	1.427 ± 0.11
calculated values ($\eta_{10} = 6.1$):	2.442 ± 0.0032	7.015 ± 0.065	1.549 ± 0.016	1.461 ± 0.11
calculated values ($\eta_{10} = 6.2$):	2.444 ± 0.0032	6.836 ± 0.065	1.532 ± 0.016	1.497 ± 0.11
calculated values ($\eta_{10} = 6.3$):	2.446 ± 0.0032	6.663 ± 0.063	1.515 ± 0.016	1.535 ± 0.11
calculated values ($\eta_{10} = 6.36515$):	2.447 ± 0.0032	6.555 ± 0.063	1.504 ± 0.016	1.562 ± 0.11
calculated values ($\eta_{10} = 6.4$):	2.448 ± 0.0032	6.497 ± 0.062	1.499 ± 0.016	1.576 ± 0.11
calculated values ($\eta_{10} = 6.5$):	2.449 ± 0.0032	6.339 ± 0.061	1.483 ± 0.016	1.618 ± 0.11
calculated values ($\eta_{10} = 6.6$):	2.451 ± 0.0032	6.186 ± 0.060	1.468 ± 0.016	1.662 ± 0.11
calculated values ($\eta_{10} = 6.7$):	2.453 ± 0.0032	6.040 ± 0.060	1.453 ± 0.016	1.708 ± 0.11
calculated values ($\eta_{10} = 6.8$):	2.454 ± 0.0032	5.899 ± 0.059	1.438 ± 0.016	1.756 ± 0.12
calculated values ($\eta_{10} = 6.9$):	2.456 ± 0.0032	5.763 ± 0.058	1.424 ± 0.016	1.806 ± 0.12
calculated values ($\eta_{10} = 7.0$):	2.458 ± 0.0032	5.633 ± 0.056	1.410 ± 0.016	1.857 ± 0.12
calculated values ($\eta_{10} = 7.1$):	2.459 ± 0.0032	5.507 ± 0.056	1.397 ± 0.016	1.910 ± 0.12
calculated values ($\eta_{10} = 7.2$):	2.461 ± 0.0032	5.386 ± 0.055	1.383 ± 0.016	1.965 ± 0.13
...	...	...	...	...